Cyclotron waves in a non-neutral plasma column

Daniel H. E. Dubin

Citation: Phys. Plasmas **20**, 042120 (2013); doi: 10.1063/1.4802101
View online: http://dx.doi.org/10.1063/1.4802101
View Table of Contents: http://pop.aip.org/resource/1/PHPAEN/v20/i4
Published by the American Institute of Physics.

Cyclotron waves in a non-neutral plasma column

Daniel H. E. Dubin
Department of Physics, University of California at San Diego, La Jolla, California 92093, USA

(Received 22 February 2013; accepted 4 April 2013; published online 25 April 2013)

A kinetic theory of linear electrostatic plasma waves with frequencies near the cyclotron frequency Ω_{c_s} of a given plasma species s is developed for a multispecies non-neutral plasma column with general radial density and electric field profiles. Terms in the perturbed distribution function up to $O(1/\Omega_{c_s}^2)$ are kept, as are the effects of finite cyclotron radius r_c up to $O(r_c^2)$. At this order, the equilibrium distribution is not Maxwellian if the plasma temperature or rotation frequency is not uniform. For $r_c \to 0$, the theory reproduces cold-fluid theory and predicts surface cyclotron waves propagating azimuthally. For finite r_c, the wave equation predicts that the surface wave couples to radially and azimuthally propagating Bernstein waves, at locations where the wave frequency equals the local upper hybrid frequency. The equation also predicts a second set of Bernstein waves that do not couple to the surface wave, and therefore have no effect on the external potential. The wave equation is solved both numerically and analytically in the WKB approximation, and analytic dispersion relations for the waves are obtained. The theory predicts that both types of Bernstein wave are damped at resonances, which are locations where the Doppler-shifted wave frequency matches the local cyclotron frequency as seen in the rotating frame. © *2013 AIP Publishing LLC*. [http://dx.doi.org/10.1063/1.4802101]

I. INTRODUCTION

This paper considers linear plasma waves near the cyclotron frequencies of a multispecies ion plasma column with near-Maxwellian velocity distributions. We focus on the z-independent component of the plasma response in the electrostatic (non-relativistic) limit, in order to simplify the analysis and make connections to experimental systems that measure this component. A broad range of devices use the electrical signal induced by this plasma response in order to diagnose the charge to mass ratio and/or the relative concentration of plasma species[1] (via the technique of "ion-cyclotron mass spectrometry"). While most of these devices work in the low-density regime where plasma effects are small, cyclotron frequency shifts universally arise from electric fields that can originate either from the plasma or potentials applied to electrodes, as will be discussed here.

Previous papers[2,3] have described theory of the electrostatic plasma response near the cyclotron frequency, in the low temperature "cold-fluid" limit, where thermal effects are not included. It was found that the cold fluid plasma response is peaked at frequencies associated with surface cyclotron waves–electrostatic plasma waves that propagate azimuthally along the surface of the plasma column as $\exp(i\ell\theta - i\omega t)$, with azimuthal mode number ℓ and frequency ω near the cyclotron frequency $\Omega_{c_s} = q_s B/m_s c$ for a given species s. The difference between ω and Ω_{c_s} arises from a Doppler shift and a Coriolis force effect due to plasma rotation, and from plasma effects proportional to the density n_s of species s. The frequency ω can then be used to diagnose the plasma rotation frequency, the density of the species, as well as the cyclotron frequency (which determines the charge to mass ratio of the species, the main interest in mass spectrometry).

In other work,[4–6] effects of finite temperature were also considered. It was observed that electrostatic Bernstein waves can be excited in addition to the cold fluid surface waves. These waves propagate both radially and azimuthally within the plasma, with frequencies that depend on the cyclotron frequency, as well as the plasma density and temperature T, which enters through the cyclotron radius $r_c = \sqrt{T/m_s}/\Omega_{c_s}$. An approximate dispersion relation for the Bernstein waves was derived in Refs. 5 and 6, based on WKB analysis.

In this paper, we present a theory of the plasma response near the cyclotron frequency, which describes both the surface cyclotron waves and the Bernstein waves in the regime $\omega_p/\Omega_{c_s} \ll 1$, where ω_p is the plasma frequency. A wave equation for the perturbed plasma potential is derived assuming $r_c/\mathcal{L} \ll 1$ and $kr_c \ll 1$ (where k is the wavenumber of the response and $\mathcal{L}$ is the radial scale length of the equilibrium plasma), which includes both the surface cyclotron and Bernstein waves as solutions. This equation is solved numerically, as well as through the WKB approximation, which is valid provided $k\mathcal{L} \gg 1$, and we extend this WKB solution through to the regime $kr_c \gtrsim 1$.

The Bernstein waves are reflected at locations where their frequency equals the plasma's upper hybrid frequency and can then set up normal modes inside the plasma column. We find that the dispersion relation for the Bernstein normal modes is modified from the qualitative result of Ref. 6 due to linear mode coupling between these modes and the electrostatic surface cyclotron waves. This coupling also allows the Bernstein modes to be observed via their effect on the external electrostatic potential, which can be picked up using electrodes. An expression is derived for the electrode signal, which can exhibit peaks at the Bernstein mode frequencies, consistent with experiments.[5] (Previous theory could not

explain this phenomenon.) This effect is similar to the linear mode coupling between electromagnetic waves and Bernstein waves that is known to occur at the upper hybrid resonance in neutral plasmas, of importance to cyclotron heating and current drive in magnetic fusion applications.[7–10] We also find a second set of Bernstein modes that do not couple to the surface cyclotron waves. These modes are internal to the plasma, having no effect on the external potential.

To derive the wave equation, we must first derive several new results for the cylindrical plasma equilibrium. First, in Sec. II, we solve for charged particle motion in the equilibrium radial electric field of the plasma, keeping finite cyclotron radius effects, which are necessary to describe the finite-temperature Bernstein modes. In so doing, we obtain finite electric field and finite cyclotron radius corrections to the particle cyclotron frequency and the drift rotation frequency. Next, in Sec. III, we obtain a closed-form expression for the collisional quasi-equilibrium velocity distribution of the rotating plasma, for given density, temperature, and radial electric field profiles, keeping finite-cyclotron radius effects. The system evolves to this quasi-equilibrium distribution due to collisions between the plasma charges. The distribution deviates from Maxwellian due to radial variations in the plasma rotation frequency and temperature; eventually on a longer "transport" timescale, these variations are wiped out by viscosity and thermal conduction, but during an intermediate timescale between the collision time and the transport time, they are present and affect the velocity distribution.

Next, in Sec. IV, we derive a general dispersion relation for linear electrostatic waves on this near-Maxwellian quasi-equilibrium by linearizing and solving the Vlasov equation with an added Krooks collision operator. The solution is obtained for general radial density, temperature, and electric field profiles. In Sec. V, we focus on the plasma response for z-independent perturbations near the cyclotron frequency of a given species, deriving the aforementioned wave equation, which keeps terms to first-order in $k^2r_c^2$. In Sec. VI, we review the cold-fluid theory of solutions to this equation (the $r_c \to 0$ limit), discussing the surface cyclotron waves that are predicted to appear under various scenarios. In Sec. VII, we add finite temperature and in Sec. VIII, we consider WKB solutions to the wave equation. In Sec. IX, we consider the behavior of the WKB solutions for a few examples.

II. PARTICLE ORBITS

Consider the orbit of a particle with charge $\pm q$ and mass m in a uniform magnetic field $\mp B\hat{z}$ and a cylindrically symmetric potential $\phi_0(r)$. Here, q and B are positive-definite quantities. For positive (negative) charges, we assume a magnetic field in the $-(+)z$ direction, so that various frequencies (cyclotron, drift rotation) are positive for either sign of charge; i.e., the resultant circular motions associated with each frequency are counter-clockwise when viewed from a location on the z axis above the orbit. The Hamiltonian for this particle, expressed in cylindrical coordinates (r, θ, z), is

$$H(\mathbf{r},\mathbf{p}) = \frac{p_r^2}{2m} + \frac{\left(p_\theta + \frac{qB}{2c}r^2\right)^2}{2mr^2} + \frac{p_z^2}{2m} + \phi_0(r), \qquad (1)$$

where $p_r = m\dot{r}, p_\theta = mr^2(\dot{\theta} - \Omega_c/2)$, and $p_z = m\dot{z}$ are the momenta canonically conjugate to r, θ, and z, respectively, and $\Omega_c = qB/mc$ is the "bare" cyclotron frequency of an isolated particle. Note that ϕ_0 has units of potential energy; it is q times the electrostatic potential. This potential can arise from voltages applied to cylindrically symmetric electrodes or from a cylindrically symmetric equilibrium distribution of plasma charges, which produces a "mean-field" equilibrium potential. In this case, H is the mean field Hamiltonian for the motion of a charge in the static field produced by the other charges. However, $\phi_0(r)$ can also arise from the interaction of a charge with its own image in the cylindrical electrodes of the trap, even in the absence of other charges.[11] This image charge potential is typically weak compared to other potentials and is often neglected, but it should be kept in high-precision work.[12] For example, for a point charge q at radius r within a hollow cylindrical conductor of radius r_w, this image potential is most easily expressed as an integral:

$$\phi_0^{\text{image}}(r) = -\frac{q^2}{r_w}\sum_{\ell=-\infty}^{\infty}\frac{2}{\pi}\int_0^\infty dx\, I_\ell^2\left(x\frac{r}{r_w}\right)\frac{K_\ell(x)}{I_\ell(x)}, \qquad (2)$$

where I_ℓ and K_ℓ are modified Bessel functions. Expressions for the image potential for other electrode geometries, both cylindrically symmetric and asymmetric, can be found in Ref. 11.

The Hamiltonian given in Eq. (1) is separable, with three constants of the motion p_θ, p_z, and $H_\perp = H - p_z^2/2m$. We will find it useful to replace the constant $H_\perp$ by the action $\mu = \frac{1}{2\pi}\oint p_r dr$, where the line integral is performed along the closed radial particle orbit. Since p_r can be expressed as a function of $H_\perp$, p_θ, and r via Eq. (1), this implies $\mu = \mu(H_\perp, p_\theta)$. Inverting this relation yields $H_\perp = H_\perp(\mu, p_\theta)$, the perpendicular Hamiltonian written in terms of the action.

When the magnetic field is large, this transformation can be accomplished perturbatively in an expansion in $1/B$ via Hamiltonian perturbation theory. This expansion requires that the cyclotron frequency associated with radial particle oscillations is large compared to the other motional frequencies, in particular the "drift" frequency associated with θ motion in the radial electric field. As a corollary, this also requires that the spatial scale length of the electric field, $\mathcal{L}$, be large compared to the cyclotron radius, so that we can perform Taylor expansions of the field around the guiding center position. (This latter requirement is sometimes violated in cyclotron mass spectrometry, where large amplitude cyclotron motion can be driven by external fields.) The result, good to order $1/B^4$, is

$$H_\perp(\mu,p_\theta) = \mu\Omega(r_0) + \phi_0(r_0) + \frac{\varepsilon^2E^2(r_0)}{2m\Omega_c^2} + \frac{\varepsilon^4E^3(r_0)}{m^2r_0\Omega_c^4} + \frac{\mu^2\varepsilon^4}{8m^2\Omega_c^2} \times\left(\frac{15}{2}\frac{E(r_0)}{r_0^3} - \frac{15}{2}\frac{E'(r_0)}{r_0^2} - 5\frac{E''(r_0)}{r_0} - \frac{1}{2}E'''(r_0)\right) + O(\varepsilon^6), \qquad (3)$$

where ε is an ordering parameter used to keep track of the order in $1/B$ of different terms, primes denote derivatives with respect to r, $E(r) = -\partial\phi_0/\partial r$, and $r_0(p_\theta)$ is the radial location of the effective potential minimum, i.e., the minimum of $\phi_0(r) + (p_\theta + qBr^2/2c)^2/2mr^2$, as given by the solution to

$$R^4 = r_0^4 - 4E(r_0)\, r_0^3/m\Omega_c^2, \tag{4}$$

where $R \equiv \sqrt{-2p_\theta c/(qB)}$, a constant of the motion (the lowest-order guiding center radius). The shifted cyclotron frequency $\Omega(r_0)$ is given by the (exact) expression

$$\Omega^2(r_0) = \Omega_c^2 - \frac{3E(r_0)}{mr_0} - \frac{E'(r_0)}{m}. \tag{5}$$

Note that the action μ appearing in Eq. (3) is of order ε. In fact, this equation implies that to lowest order in ε, $\mu \approx \varepsilon\, m\mathrm{v}_\perp^2/2\Omega_c$, the well-known expression for the cyclotron action. Also, Eq. (5) shows that the cyclotron frequency is shifted by the radial electric field. In experiments with low plasma density or even single particles, the shift arises predominantly from applied trap potentials and/or image charges. In this paper, we obtain frequency shifts to collective plasma modes (as well as single particle frequencies), including plasma effects, applied potentials, and image charges.

The transformation from $(r, p_r, \theta, p_\theta)$ to the action-angle variables $(\psi, \mu, \bar\theta, p_\theta)$ used in Eq. (3) can be carried out with generating functions W_r and W_θ where[13]

$$W_\theta \equiv p_\theta\theta, \tag{6}$$

$$W_r(r, \mu, p_\theta) \equiv \int^r p_r(r, H_\perp, p_\theta), \tag{7}$$

and we have used $H_\perp = H_\perp(\mu, p_\theta)$. These generating functions relate the new and old coordinates via

$$\psi = \frac{\partial}{\partial\mu}(W_r + W_\theta) = \frac{\partial W_r}{\partial\mu}(r, \mu, p_\theta). \tag{8}$$

Inverting, this yields

$$r = r(\psi, \mu, p_\theta) \equiv r_0 + \delta r(\psi, \mu, p_\theta), \tag{9}$$

where the second form is actually a definition of δr, the deviation of r from r_0 due to finite cyclotron radius effects. Also, we have

$$\bar\theta = \frac{\partial}{\partial p_\theta}(W_r + W_\theta) = \theta + \frac{\partial W_r}{\partial p_\theta}(r, \mu, p_\theta), \tag{10}$$

which we can rearrange as

$$\theta = \bar\theta + \delta\theta(\psi, \mu, p_\theta), \tag{11}$$

where

$$\delta\theta(\psi, \mu, p_\theta) = -\frac{\partial W_r}{\partial p_\theta}(r(\psi, \mu, p_\theta), \mu, p_\theta). \tag{12}$$

Perturbation analysis, described in Appendix A, provides us with explicit expressions for δr and $\delta\theta$:

$$\delta r = \sum_{n=0}^{\infty} \varepsilon^n \Delta r_n(\rho, r_0, \varepsilon)\cos n\psi, \tag{13}$$

$$\delta\theta = \sum_{n=1}^{\infty} \varepsilon^n \Delta\theta_n(\rho, r_0, \varepsilon)\sin n\psi. \tag{14}$$

Here, Δr_n and $\Delta\theta_n$ are given as power series in ε up to $O(\varepsilon^4)$ in Table I, and $\rho^2 \equiv 2\mu/m\Omega_c$. The parameter ρ is, to lowest order in $1/B$, the radius of the cyclotron orbit. The coefficient Δr_0 is the radial change in guiding center position due to finite cyclotron radius effects. Note that for $n \geq 1$, both Δr_n and $\Delta\theta_n$ enter δr and $\delta\theta$ at $O(\varepsilon^n)$.

The inverse of these transformations can also be written as power series in ε. In particular, $\mu(r, \mathrm{v}_r, \mathrm{v}_\theta)$ is given by

$$\mu = \varepsilon m\frac{\mathrm{v}_r^2 + \mathrm{v}_\theta^2}{2\Omega_c} - \varepsilon^2\mathrm{v}_\theta\frac{E(r)}{\Omega_c^2} + \varepsilon^3 \times \frac{m\mathrm{v}_\theta^2(E(r) + 3rE'(r)) + m\mathrm{v}_r^2(3E(r) + rE'(r)) + 2rE(r)^2}{4mr\Omega_c^2} + O(\varepsilon^4). \tag{15}$$

The Hamiltonian of Eq. (3) implies that the angle variables $\bar\theta$ and ψ, and the coordinate z evolve in time according to

$$\frac{d\psi}{dt} = \frac{\partial H_\perp}{\partial\mu} = \bar\Omega(r_0, \rho), \tag{16}$$

$$\frac{d\bar\theta}{dt} = \frac{\partial H_\perp}{\partial p_\theta} = \bar\omega_0(r_0, p), \tag{17}$$

$$\frac{dz}{dt} = \frac{\partial H}{\partial p_z} = \frac{p_z}{m}, \tag{18}$$

where the frequencies $\bar\Omega$ and $\bar\omega_0$ are given by the series expressions

TABLE I. Orbit coefficients in Eqs. (13) and (14).

n	Δr_n
0	$\frac{3}{4}\frac{\varepsilon^2\rho^2}{4r_0} - \frac{15}{64}\frac{\varepsilon^4\rho^4}{r_0^3} + \frac{\varepsilon^4\rho^2}{m\Omega_c^2}\left(\frac{3}{8}\frac{E(r_0)}{r_0^2} + \frac{9}{8}\frac{E'(r_0)}{r_0} + \frac{1}{4}E''(r_0)\right) + O(\varepsilon^6)$
1	$\rho + \varepsilon^2\left(\frac{-\rho^3}{8r_0^2} + \frac{\rho}{m\Omega_c^2}\left(\frac{3}{4}\frac{E(r_0)}{r_0} + \frac{1}{4}E(r_0)\right)\right) + O(\varepsilon^4)$
2	$-\frac{\rho^2}{4r_0} + \varepsilon^2\left(\frac{3}{16}\frac{\rho^4}{r_0^3} - \frac{\varepsilon^2\rho^2}{m\Omega_c^2}\left(\frac{1}{8}\frac{E(r_0)}{r_0^2} + \frac{3}{8}\frac{E'(r_0)}{r_0} + \frac{1}{12}E''(r_0)\right)\right) + O(\varepsilon^4)$
3	$\frac{\rho^3}{8r_0^2} + O(\varepsilon^2)$
4	$-\frac{5}{64}\frac{\rho^4}{r_0^3} + O(\varepsilon^2)$
n	$\Delta\theta_n$
1	$\frac{\rho}{r_0} + \varepsilon^2\left(-\frac{1}{2}\frac{\rho^3}{r_0^3} + \frac{\rho}{r_0}\frac{E(r_0)+3r_0E'(r_0)}{4mr_0\Omega_c^2}\right) + O(\varepsilon^4)$
2	$-\frac{\rho^2}{2r_0^2} + \varepsilon^2\left(\frac{1}{2}\frac{\rho^4}{r_0^4} - \frac{\rho^2}{8r_0^2}\frac{3E(r_0)+5r_0E'(r_0)+r_0^2E''(r_0)/3}{mr_0\Omega_c^2}\right) + O(\varepsilon^4)$
3	$\frac{\rho^3}{3r_0^3} + O(\varepsilon^2)$
4	$-\frac{\rho^4}{4r_0^4} + O(\varepsilon^2)$

$$\bar{\Omega}(r_0,\rho) = \frac{\Omega(r_0)}{\varepsilon} + \frac{\varepsilon^3\rho^2}{8m\Omega_c} \times \left(\frac{15}{2}\frac{E(r_0)}{r_0^3} - \frac{15}{2}\frac{E'(r_0)}{r_0^2} - \frac{5E''(r_0)}{r_0} - \frac{1}{2}E'''(r_0)\right) + O(\varepsilon^5), \tag{19}$$

$$\bar{\omega}_0(r_0,\rho) = \frac{dr_0}{dp_\theta}\frac{\partial H}{\partial r_0}\bigg|_{\mu,p_z} = \varepsilon\omega_E(r_0) + \frac{\varepsilon^3\omega_E(r_0)^2}{\Omega_c} - \frac{\varepsilon^3\rho^2}{4m\Omega_c r_0} \times \left(\frac{3E(r_0)}{r_0^2} - \frac{3E'(r_0)}{r_0} - E''(r_0)\right) + O(\varepsilon^5), \tag{20}$$

and where

$$\omega_E(r_0) \equiv \frac{E(r_0)}{m\Omega_c r_0}. \tag{21}$$

The drift rotation frequency $\bar{\omega}_0$ is, to lowest order in $1/B$, given by the $E\times B$ drift rotation frequency ω_E in the radial electric field. The second term in Eq. (20) is a correction due to centrifugal force, which acts as an extra radial force that causes an $F\times B$ drift in the θ-direction. The terms proportional to ρ^2 are finite cyclotron radius corrections to the rotation rate.

The cyclotron frequency $\bar{\Omega}$ also has finite cyclotron radius corrections. However, when comparing this expression to previous expressions for the cyclotron frequency in the presence of an electric field,[14] it is important to remember that here the frequency is derived as the rate of radial oscillations, which is not the same as the cyclotron rotation rate with respect to fixed Cartesian axes since the direction of the radial unit vector varies in time as the particle moves in θ. Thus, single particle resonances can be shifted from the cyclotron frequency $\bar{\Omega}$ by (multiples of) the rotation frequency $\bar{\omega}_0$. In fact, when subjected to external fields varying in r, θ, and t as $\delta\phi(r)e^{i\ell\theta-i\omega t}$, we will see that particles can absorb energy resonantly when the applied fields are at the frequencies $\omega = n\bar{\Omega} + \ell\bar{\omega}_0$ for any integer n. The resonant interaction with $n=1$ at a frequency near $\bar{\Omega}$ is typically the strongest resonance and is the main effect observed in ion-cyclotron mass spectrometry for low density systems. However, for higher densities, there are collective electrostatic plasma waves that can be excited. These collective excitations are the subject of the next sections.

One type of system for which these frequency formulae simplify is the harmonic trap where to a good approximation (and neglecting z dependence, valid for particles moving in the $z=0$ plane), $\phi_0(r)\propto r^2$. Then, the finite cyclotron radius corrections to $\bar{\Omega}$ and $\bar{\omega}_0$ vanish in Eqs. (19) and (20), and these frequencies are independent of radial position, which simplifies the analysis. This is one reason why harmonic traps are often preferred in ion-cyclotron spectrometry applications. (For a harmonic trap, our frequencies $\bar{\Omega}$ and $\bar{\omega}_0$ are related to the standard harmonic trap frequencies ω_+ and ω_-,[15] via the formulae $\bar{\omega}_0=\omega_-$ and $\bar{\Omega}=\omega_+-\omega_-$.) Of course, even in traps designed so that the vacuum field is harmonic, effects such as plasma space charge and image charges can add anharmonic corrections to ϕ_0, necessitating inclusion of the frequency corrections described by Eqs. (19) and (20).

III. EVOLUTION OF THE DISTRIBUTION FUNCTION

We assume that the particle distribution $f(\mathbf{r},\mathbf{v},t)$ for a single species plasma evolves according to the Boltzmann equation

$$\frac{\partial f}{\partial t} + \mathbf{v}\cdot\nabla f + \frac{q}{m}\left(\mathbf{E} + \frac{\mathbf{v}\times\mathbf{B}}{c}\right)\cdot\frac{\partial f}{\partial \mathbf{v}} = C(f,f), \tag{22}$$

where C is the 2 particle Boltzmann collision operator.

We first consider the cylindrically symmetric quasi-equilibrium distribution predicted by Eq. (22). Neglecting collisions, the collisionless Boltzmann equation has time-independent solutions of the general form

$$f = f_0(\mu,p_\theta,p_z) \tag{23}$$

since μ, p_θ, and p_z are constants of the collisionless motion described by Eq. (1). Any function of these constants of the motion is a collisionless (Vlasov) equilibrium. However, when collisions are taken into account, this distribution evolves on the timescale of the collision rate to a quasi-equilibrium near-Maxwellian distribution whose dependence on the constants of motion is determined by the collision operator.[16] However, the temperature, density, and rotation rate of the equilibrium can have arbitrary radial dependence. [This quasi-equilibrium then proceeds to evolve in time on a slower "transport" timescale due to radial fluxes driven by gradients in the plasma rotation frequency and the plasma temperature, toward a thermal equilibrium state with no such gradients. We neglect this slow evolution here.] The derivation of the quasi-equilibrium distribution function is outlined in Appendix B. Assuming that the temperature gradient is of order ε^2 while density and rotation frequency gradients are of $O(1)$, the quasi-equilibrium is, to $O(\varepsilon^4)$,

$$f_{qe}(\mu,p_\theta,p_z) = \frac{N(R)}{(2\pi T(R)/m)^{3/2}}\exp\{-H/T(R) - \mu\Omega_c(1/T_\mu(R) - 1/T(R)) + O(\varepsilon^4)\}, \tag{24}$$

where $R\equiv\sqrt{-2p_\theta/m\Omega_c} = \sqrt{r^2 - 2rv_\theta/\Omega_c}$ is the lowest-order guiding center radius [see Eq. (4)], the function $N(R)$ is related to equilibrium density $n(r)$ and potential $\phi_0(r)$,

$$N(R) \equiv n(R)\exp\{[\phi_0(R) - 1/2mR^2\varepsilon^2\omega_r^2(R)]/T(R)\}, \tag{25}$$

the cyclotron temperature $T_\mu(R)$ is related to the parallel temperature $T(R)$ through

$$T_\mu(R) \equiv T(R)\left(1 + \frac{\varepsilon^2 R}{2\Omega_c}\frac{\partial\omega_r}{\partial R}\right), \tag{26}$$

and $\omega_r(R)$ is the fluid rotation frequency, defined as

$$r\,n(r)\omega_r(r) = \int d^3\mathrm{v}\,\mathrm{v}_\theta f_{qe}. \tag{27}$$

[Note that in these velocity integrals, r is held fixed, not R. The expression for f_{qe} given in Eq. (B25), while less elegant than Eq. (24), is easier to integrate over velocities.] Performing the velocity integrals yields the following expression for ω_r up to $O(\varepsilon^3)$:

$$\omega_r(r) = \frac{\varepsilon}{m\Omega_c r}\left[-\frac{1}{n}\frac{\partial}{\partial r}(T(r)n(r)) + E(r)\right] + \varepsilon^3 \times \left[\frac{\omega_r^2}{\Omega_c} - \frac{T}{2m\Omega_c^2 r}\left(\frac{r}{n}\frac{\partial n}{\partial r} + 3\right)\frac{\partial \omega_r}{\partial r} - \frac{T}{2m\Omega_c^2}\frac{\partial^2\omega_r}{\partial r^2}\right] + O(\varepsilon^5). \tag{28}$$

The lowest order fluid rotation frequency in Eq. (28) is the familiar expression for diamagnetic and $E\times B$ drifts.[17] The $O(\varepsilon^3)$ corrections are due to centrifugal force (the first term) and thermally averaged finite cyclotron radius corrections due to shear in the fluid rotation (the 2nd and 3rd terms). Although ω_r appears on both sides of this expression, to $O(\varepsilon^3)$ one can use the lowest-order drift expression for ω_r on the right hand side to obtain an explicit expression for ω_r in terms of density, potential, and temperature.

When T and ω_r are uniform (independent of r), Eq. (24) reduces to the thermal-equilibrium form

$$f_{qe} = \frac{N_0}{(2\pi T/m)^{3/2}} e^{-H/T+\omega_r p_\theta/T}, \tag{29}$$

where N_0 is a constant. This can be seen by noting that, when ω_r and T are constant, Eqs. (25) and (28) imply that

$$-\frac{T}{m\Omega_c RN}\frac{\partial N}{\partial R} = \omega_r, \tag{30}$$

which implies that in thermal equilibrium, $N(R) = N_0 e^{\omega_r p_\theta/T}$. When applied to Eq. (24), this leads to Eq. (29).

However, when T and/or ω_r are not uniform, Eq. (24) is not a Maxwellian distribution due to the dependence of R on v_θ. Collisions drive the system "as close to a Maxwellian as possible" when variations in ω_r and T are present. The non-Maxwellian nature of f_{qe} is responsible for the difference between cyclotron temperature T_μ and parallel temperature T. With the definition of T_μ given by Eq. (26), the mean kinetic energy per particle in each degree of freedom, as determined by velocity integration over f_{qe}, is given by

$$\langle m\mathrm{v}_r^2\rangle = T(r)\left(1 + \frac{\varepsilon^2 r}{2\Omega_c}\frac{\partial\omega_r}{\partial r} + O(\varepsilon^4)\right), \tag{31}$$

$$\langle m(\mathrm{v}_\theta - \omega_r r)^2\rangle = T(r)\left(1 - \frac{\varepsilon^2 r}{2\Omega_c}\frac{\partial\omega_r}{\partial r} + O(\varepsilon^4)\right), \tag{32}$$

and

$$\langle m\mathrm{v}_z^2\rangle = T(r). \tag{33}$$

Thus, the mean transverse thermal energy $\langle 1/4\, m(\mathrm{v}_r^2 + (\mathrm{v}_\theta - \omega_r r)^2)\rangle$ is equal to the mean parallel thermal energy $\langle m\mathrm{v}_z^2/2\rangle$. This is required in quasi-equilibrium; otherwise there will be equipartition of parallel and perpendicular thermal energy on a collisional timescale. (Note that the differences in mean radial, axial, and azimuthal thermal energy could, in principle, be observed using, say, laser doppler diagnostics.)

IV. GENERAL DISPERSION RELATION FOR LINEAR WAVES

We now consider small perturbations $\delta f_s(\mathbf{r},\mathbf{v},t)$ of $f_s(\mathbf{r},\mathbf{v},t)$ away from the quasi-equilibrium f_{qe_s} given by Eq. (24). Here, we re-introduce a species label s for species with mass m_s and charge q_s. The perturbations are described by linearization of the multispecies version of the Boltzmann equation, Eq. (22). For simplicity, we use a simple Krook collision operator of the form $C = -\nu(f_s - f_{qe_s})$. Substituting

$$f_s = f_{qe_s} + \delta f_s(\mathbf{r},\mathbf{v},t) \tag{34}$$

and

$$\phi = \phi_0(r) + \delta\Phi(\mathbf{r},t) \tag{35}$$

into Eq. (22) and linearizing, we obtain

$$\frac{d}{dt}\delta f_s + \nu\delta f_s = \frac{\partial f_{qe_s}}{\partial\mu}\frac{\partial\delta\Phi}{\partial\psi} + \frac{\partial f_{qe_s}}{\partial p_\theta}\frac{\partial\delta\Phi}{\partial\bar{\theta}} + \frac{\partial f_{qe_s}}{\partial p_z}\frac{\partial\delta\Phi}{\partial z}, \tag{36}$$

where

$$\frac{d}{dt} = \frac{\partial}{\partial t} + \mathbf{v}\cdot\nabla + \left(\frac{E(r)}{m}\hat{r} - \mathbf{v}\times\hat{z}\Omega_{c_s}\right)\cdot\frac{\partial}{\partial\mathbf{v}} \tag{37}$$

is a derivative taken along the orbit of the Hamiltonian of Eq. (1). The right-hand side of Eq. (36) is written in terms of action-angle variables.

Next, we Fourier analyze δf and $\delta\Phi$ in θ, z, and t, writing these functions as

$$\delta f_s(\mathbf{r},\mathbf{v},t) = \delta F_s(r,\mathbf{v})\, e^{i\ell\theta + ik_z z - i\omega t} \tag{38}$$

and

$$\delta\Phi(\mathbf{r},t) = \delta\phi(r)\, e^{i\ell\theta + ik_z z - i\omega t}. \tag{39}$$

Applying Eqs. (9) and (11), we define

$$\delta\phi(r_0+\delta r)\, e^{i\ell\delta\theta} \equiv \sum_{n=-\infty}^{\infty}\Delta\phi_{\ell n}(p_\theta,\mu)\, e^{in\psi}, \tag{40}$$

where the $\Delta\phi_{\ell n}$ are the Fourier coefficients of the left-hand side, which is periodic in ψ [see Eqs. (13) and (14)]. We may then integrate Eq. (36), obtaining

$$e^{i\ell\theta + ik_z z - i\omega t}\delta F_s(r,\mathrm{v}_r,\mathrm{v}_\theta,\mathrm{v}_z) = \sum_{n=-\infty}^{\infty}\Delta\phi_{\ell n}(p_\theta,\mu)\left(in\frac{\partial f_{qe}}{\partial\mu} + i\ell\frac{\partial f_{qe}}{\partial p_\theta} + ik_z\frac{\partial f_{qe}}{\partial p_z}\right) \times e^{-\nu t}\int_{-\infty}^{t} dt'\, e^{in\psi(t') + i\ell\bar{\theta}(t') + ik_z z(t') - i(\omega+i\nu)t'}, \tag{41}$$

where $\psi(t'), \bar{\theta}(t')$, and $z(t')$ are determined by the equations of motion (16)–(19)

$$\psi(t') = \psi_0 + \bar{\Omega}_s(r_0, \rho)(t' - t), \tag{42a}$$

$$\bar{\theta}(t') = \theta_0 + \bar{\omega}_{0_s}(r_0, \rho)(t' - t), \tag{42b}$$

$$z(t') = z + \mathrm{v}_z(t' - t). \tag{42c}$$

Here, the constants of integration ψ_0 and θ_0 and the constant of motion μ are determined in terms of r, θ, v_r, and v_θ by the conditions

$$\theta_0 + \delta\theta(\psi_0, r_0, \rho) = \theta, \tag{43}$$

$$r_0 + \delta r(\psi_0, r_0, \rho) = r, \tag{44}$$

$$\delta\dot{r}(\psi_0, r_0, \rho) = \mathrm{v}_r. \tag{45}$$

Equations (44) and (45) determine ψ_0 and μ using Eqs. (4) and (13), and then Eq. (43) determines θ_0. Note that no equation for v_θ is necessary since v_θ is determined in terms of r and p_θ by $p_\theta = m\mathrm{v}_\theta r - qBr^2/2c$. Of course, μ is also determined by r, v_r, and v_θ via Eq. (15).

Using Eqs. (42) in Eq. (41), the time integral can be performed, yielding

$$\delta F_s(r, \mathrm{v}_r, \mathrm{v}_\theta, \mathrm{v}_z) = \sum_{n=-\infty}^{\infty} e^{-i\ell\delta\theta(\psi_0, r_0, \rho) + in\psi_0} \Delta\phi_{\ell n}(p_\theta, \mu) \times \frac{n\dfrac{\partial f_{qe_s}}{\partial \mu} + \ell\dfrac{\partial f_{qe_s}}{\partial p_\theta} + k_z\dfrac{\partial f_{qe_s}}{\partial p_z}}{n\bar{\Omega}_s(r_0, \rho) + \ell\bar{\omega}_{0_s}(r_0, \rho) + k_z\mathrm{v}_z - \omega - i\nu}. \tag{46}$$

The resonant denominator in Eq. (46) provides an expression for the frequency ω at which there is a strong wave-particle resonant interaction, as we discussed at the end of Sec. II.

Finally, the dispersion relation for $\delta\phi$ is obtained by substituting Eqs. (38) and (39) into Poisson's equation

$$\frac{1}{r}\frac{\partial}{\partial r} r \frac{\partial \delta\phi(r)}{\partial r} - \left(\frac{\ell^2}{r^2} + k_z^2\right)\delta\phi(r) = -4\pi e^2 \sum_s \int d^3\mathrm{v}\, \delta F_s(r, \mathrm{v}_r, \mathrm{v}_\theta, \mathrm{v}_z). \tag{47}$$

This integro-differential equation for $\delta\phi$ can be solved subject to the boundary conditions on $\delta\phi$. With regard to Eqs. (46) and (47), we note that the derivatives with respect to μ and p_θ are easiest to evaluate using the form of f_{qe_s} given in Eq. (24), but the velocity integrals are easiest to evaluate using the equivalent form given in Eq. (B25).

V. CYCLOTRON MODES FOR SPECIES *s*

We focus on z-independent cyclotron modes, assuming $k_z = 0$. There are cyclotron modes near multiples n of the cyclotron frequency for each species. In this paper, we consider only the modes for which $n = 1$, near the cyclotron frequency Ω_{c_s} of species s, with $\omega = \Omega_{c_s} + O(\varepsilon)$. Substituting Eq. (24) [or Eq. (B25)] for f_{qe_s} into Eq. (47), expanding the integrand in ε, and carrying out the velocity integrals, we keep enough terms in the series expressions so that finite temperature corrections to the dispersion relation are obtained. These corrections enter at $O(\varepsilon^2)$, so, noting that $\bar{\omega}_0 = O(\varepsilon)$ and $\Delta\phi_{\ell n} = O(\varepsilon^n)$ for $n \neq 0$, analysis of Eq. (47) implies that terms in the sum over n in δF_s can be dropped only for $|n| > 2$ that f_{qe_s} must be evaluated including terms up to $O(\varepsilon^3)$ and that $\Delta\phi_{\ell n}$ must be evaluated up to $O(\varepsilon^4)$. The perturbed density for species s can then be evaluated by performing the velocity integral over δF_s

$$\int d^3\mathrm{v}\delta F_s = \delta n_{F_s}(r) + \delta n_{T_s}(r), \tag{48}$$

where $\delta n_{F_s}(r)$ is the $T = 0$ "cold fluid" density response to the perturbed potential $\delta\phi$, and $\delta n_{T_s}(r)$ is the $T > 0$ thermal correction. The cold fluid density perturbation can also be derived directly to all orders in ε from fluid equations[6] and has the form

$$4\pi q_s^2 \delta n_{F_s}(r) = -\frac{\ell}{r}\frac{\omega_{p_s}^2(r)}{\hat{\omega}} \frac{(\Omega_{\mathrm{v}s} - r\omega'_{F_s}(r))\delta\phi'(r) + \ell(\hat{\omega} + i\nu)\delta\phi/r}{\Omega_{\mathrm{v}_s}(\Omega_{\mathrm{v}_s} - r\omega'_{F_s}(r)) - (\hat{\omega} + i\nu)^2} + \frac{1}{\hat{\omega} r}\frac{\partial}{\partial r}\left[r\omega_{p_s}^2(r)\frac{\ell\Omega_{\mathrm{v}_s}\delta\phi/r + (\hat{\omega} + i\nu)\delta\phi'(r)}{\Omega_{\mathrm{v}_s}(\Omega_{\mathrm{v}_s} - r\omega'_{F_s}(r)) - (\hat{\omega} + i\nu)^2}\right], \tag{49}$$

where $\hat{\omega} \equiv \omega - \ell\omega_{F_s}(r)$ is the Doppler-shifted frequency, $\Omega_{\mathrm{v}_s} \equiv \Omega_{c_s} - 2\omega_{F_s}$, $\omega_{p_s}^2(r) \equiv 4\pi q_s^2 n_s(r)/m_s$ is the square of the species s plasma frequency, and $\omega_{F_s}(r)$ is the cold-fluid rotation frequency given by the solution to the equation $2\omega_{F_s}(\Omega_{c_s} - \omega_{F_s}) = \sum_s \omega_{p_s}^2(r)$. However, the velocity integral in Eq. (47) yields an expansion in ε of this general expression, including terms of $O(\varepsilon^2)$:

$$4\pi q_s^2 \delta n_{F_s}(r) = \frac{1}{r}\frac{\partial}{\partial r}(r(D-1)u(r)) - (D-1)\frac{\ell u}{r} + O(\varepsilon^2), \tag{50}$$

where the field amplitude $u(r)$ is defined as

$$u(r) \equiv \delta\phi'(r) + \ell\delta\phi/r, \tag{51}$$

$$D(r) \equiv 1 - \frac{\beta(r)}{\alpha(r)} \tag{52}$$

is the dielectric constant for the species s cyclotron modes,

$$\alpha(r) \equiv \omega - \Omega_{c_s} + (2 - \ell)\omega_E + r\omega'_E(r)/2 + i\nu \tag{53}$$

is a frequency "offset", and

$$\beta(r) \equiv \frac{\omega_{p_s}^2(r)}{2\Omega_{c_s}} \tag{54}$$

represents the local species density $n_s(r)$, expressed as the equivalent $E \times B$ rotation rate for a *uniform* n_s. We do not display the $O(\varepsilon^2)$ terms in the cold fluid density perturbation as they are fairly complex and will not be needed in what follows. The frequency offset α is, in fact, (the negative of) the

resonant denominator that appears in Eq. (46) for $\Omega = 1$, expanded to lowest order in ε with the assumption that $\omega = \Omega_{c_s} + O(\varepsilon)$. This implies that α is also of $O(\varepsilon)$.

Next, we consider the thermal density correction for species s, which takes the form

$$4\pi q_s^2 \delta n_{T_s}(r) = -r_c^2\left(C_1 + \frac{C_2}{\alpha^2} + \frac{C_3}{\alpha^3} + \frac{C_4}{\alpha^4}\right), \tag{55}$$

where

$$C_1 = \nabla_\ell^2\left(\frac{\beta}{\alpha}\nabla_\ell^2\delta\phi\right) + 2\frac{\ell-1}{r}\left(\frac{\partial}{\partial r} - \frac{\ell}{r}\right)\frac{\beta' u}{\alpha}, \tag{56}$$

$$\begin{aligned} C_2 = {} & \frac{\omega_E'}{r}\ell(\ell-1)\left[\frac{\partial}{\partial r} + \frac{(\ell-5)}{r}\right]\beta u \\ & + \alpha'\left[\frac{2\ell^2-\ell}{r^2}\beta u + \frac{\ell-2}{r}\beta' u - \frac{\beta u'}{r} - \beta' u' - \beta'' u\right] \\ & - \alpha''\left[2\beta' u + \beta u' - \frac{(\ell-2)}{r}\beta u\right] - \alpha'''\beta u, \end{aligned} \tag{57}$$

$$\begin{aligned} C_3 = {} & \alpha'^2\left[\beta u' + 3\beta' u + (3-\ell)\frac{\beta u}{r}\right] \\ & + 2\alpha'\left[2\alpha'' - \omega_E'\frac{\ell(\ell-1)}{r}\right]\beta u, \end{aligned} \tag{58}$$

$$C_4 = -3\alpha'^3\beta u, \tag{59}$$

where

$$\nabla_\ell^2 \equiv \frac{1}{r}\frac{\partial}{\partial r}r\frac{\partial}{\partial r} - \frac{\ell^2}{r^2}. \tag{60}$$

Finally, we note that Eq. (49) implies that for a different species $\bar{s} \neq s$ with $\Omega_{c\bar{s}} - \Omega_{c_s} = O(1/\varepsilon)$, $\delta n_{F\bar{s}} = O(\varepsilon^2)$. Also, we find the thermal corrections to $\delta n_{\bar{s}}$ are even higher order in ε. We, therefore, neglect $\delta n_{\bar{s}}$ when solving Eq. (47), so only the density perturbation for species s need be kept for species s cyclotron waves.

Furthermore, since Eqs. (60) and (51) imply

$$\nabla_\ell^2\delta\phi = \frac{1}{r}\frac{\partial}{\partial r}(ru) - \frac{\ell u}{r}, \tag{61}$$

the thermal density correction for species s can be written entirely in terms of u and its derivatives up to third order. Thus, Eq. (47) combined with Eqs. (48), (50) and (55) constitute a third-order ordinary differential equation (ODE) for $u(r)$, which must be solved subject to the boundary conditions for $\delta\phi$.

While the ODE is fairly complex, its form can be tested in various ways. For instance, the thermal corrections, proportional to r_c^2, enter as expected from analysis for a homogeneous system, i.e., $\delta n_{T_s} = -n_s k^4 r_c^2 \delta\phi/(2m_s\Omega_{c_s}\alpha)$.[18] Also for the case $\ell = 1$ in a single species plasma, a simple analytic solution exists[6]

$$\delta\phi(r) = Ar[\omega + i\nu - \Omega_{c_s} + \omega_E(r)], \tag{62}$$

due to the fact that this excitation is a center-of-mass oscillation in which the entire column is displaced, and thermal effects on the density perturbation must vanish as a consequence. Indeed, substitution of Eq. (51) and (62) into Eq. (55) for $\ell = 1$, along with the Poisson equation relating total charge density $\rho_{\rm tot} = \sum_s q_s n_s$ to $E \times B$ rotation frequency,

$$\rho_{\rm tot}(r) = \frac{B}{4\pi c r}\frac{\partial}{\partial r}(r^2\omega_E), \tag{63}$$

yields $\delta n_{T_s} = 0$ if there is only one species, so that $\rho_{\rm tot} = q_s n_s$. Furthermore, the cold-fluid density perturbation satisfies $\nabla^2\delta\phi + 4\pi q_s^2\delta n_{F_s} = 0$, showing that Eq. (62) is a solution of Eq. (47) for $\ell = 1$ in a single species plasma.

Furthermore, if ω is chosen as $\omega = \Omega_{c_s} - \omega_E(r_w) - i\nu$, Eq. (62) implies that the perturbed potential at r_w vanishes. This is the frequency of the $\ell = 1$ "center of mass" cyclotron eigenmode in a single species plasma column [correct to $O(\varepsilon)$]. The frequency shift $\omega_E(r_w)$ is caused by $E \times B$ rotation of the center of mass in the plasma's image charge electric field.

VI. COLD FLUID THEORY OF SURFACE CYCLOTRON MODES

In the zero-temperature "cold-fluid" limit, the cyclotron mode dispersion relation becomes

$$\nabla^2\delta\phi + 4\pi q_s^2\delta n_{F_s} = 0, \tag{64}$$

with δn_{F_s} given by Eq. (50). Following Gould,[6] we will solve this equation for $\delta\phi(r)$ using the related field amplitude $u(r)$. Using Eqs. (50) and (61), Eq. (64) can be written as a first-order ODE for $u(r)$,[6]

$$\frac{1}{r}\frac{\partial}{\partial r}(rDu) - \frac{\ell}{r}Du = 0. \tag{65}$$

The solution of this equation is

$$u(r) = Ar^{\ell-1}/D(r), \tag{66}$$

where the constant A is determined by boundary conditions on $\delta\phi(r)$. We will consider the following boundary conditions

$$\delta\phi(r_w) = \phi_w; \quad \delta\phi(r_{\rm in}) = 0, \quad 0 \le r_{\rm in} < r_w. \tag{67}$$

For the special case $\ell \le 0$ and $r_{\rm in} = 0$, the 2nd boundary condition must be modified to $\delta\phi(0) =$ finite.

The first boundary condition corresponds to a potential of magnitude ϕ_w applied to an exterior electrode of radius r_w, oscillating in time at frequency ω; and the second boundary condition corresponds to an inner conductor of radius $r_{\rm in}$ at fixed voltage (see Fig. 1). Taking $r_{\rm in} = 0$ (by which we mean no interior conductor) is typical in many experiments.

The equilibrium density of a given species s, $n_s(r)$, can have arbitrary radial dependence, but in most experiments, $\omega_E(r)$ is monotonically decreasing; otherwise, the plasma can be unstable.[26] The $E \times B$ rotation frequency is determined by the total charge density $\rho_{\rm tot}$ through Eq. (63) (see Fig. 1). The density of species s need not have the same profile shape as $\rho_{\rm tot}(r)$ since various forces act differently on different species and can even produce centrifugal or charge

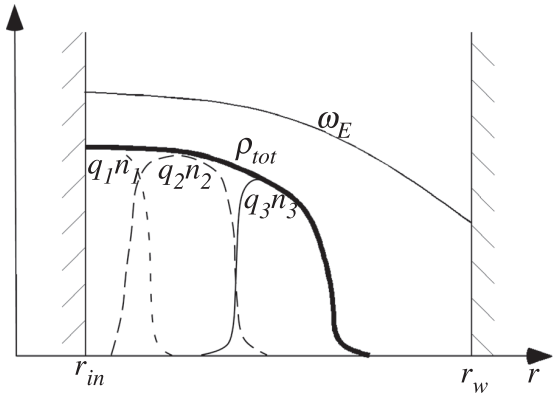

FIG. 1. Schematic diagram of the charge densities and $E \times B$ rotation frequency ω_E in a non-neutral plasma column consisting of three species. Cylindrical conductors bound the plasma at $r_{\rm in}$ and r_w; in many experiments, the inner conductor is not present. Centrifugal and/or charge separation[25] can cause the species to separate radially, in order of largest to smallest charge to mass ratio.

separation of the species densities at sufficiently low temperature and large ω_E.[25] We will find that there are surface cyclotron waves that propagate along the edge(s) of each species' density profile, producing measurable electric fields at the walls. When there is no inner conductor, there is also a second set of internal upper hybrid waves that do not affect the potential outside the plasma.

With the boundary condition $\delta\phi(r_{\rm in}) = 0$, Eq. (51) implies

$$\delta\phi(r) = r^{-\ell}\int_{r_{\rm in}}^{r} dr' r'^{\ell} u(r'). \tag{68}$$

For the special case $r_{\rm in} = 0$ (no interior conductor), this must be modified to

$$\delta\phi(r) = r^{-\ell}\left[C + \int_0^r dr' r'^{\ell} u(r')\right]. \tag{69}$$

For $\ell \le 0$, the constant C is undetermined, but for $\ell > 0$, we require that $C = 0$ so that $\delta\phi$ remains finite at $r = 0$.

A. Upper hybrid cutoff

For any ℓ, a possible solution of Eq. (65) is $Du = 0$. This corresponds to a localized upper-hybrid oscillation with $u = B\delta(r - r_{\rm UH})$, at any location $r_{\rm UH}$ for which $D(r_{\rm UH}) = 0$, which can be written as $\alpha(r_{\rm UH}) = \beta(r_{\rm UH})$ using Eq. (52). In the theory of electromagnetic wave propagation, such locations are referred to as upper hybrid resonances,[18] but for the electrostatic Bernstein waves discussed in this paper, these locations act as cutoffs, reflecting the waves. We, therefore, refer to a location where $\alpha = \beta$ as an upper hybrid cutoff. Using Eqs. (53), (52), and (63), the frequency at cutoff can be written as

$$\omega + i\nu - \Omega_{c_s} = (\ell - 1)\omega_E(r_{\rm UH}) - \sum_{\bar{s}\neq s}\frac{\omega_{p\bar{s}}{}^2(r_{\rm UH})}{2\Omega_{c_s}}. \tag{70}$$

This is the expression for the upper hybrid frequency in a rotating plasma column, in the low density limit $\omega_{p_s}/\Omega_{c_s} \ll 1$. At $r_{\rm UH}$, $u(r)$ is undefined, but it is zero everywhere else.

The potential corresponding to these upper hybrid oscillations is, according to Eq. (69),

$$\delta\phi = Cr^{-\ell} + \begin{cases} 0, & r < r_{\rm UH} \\ B(r_{\rm UH}/r)^{\ell}, & r > r_{\rm UH}, \end{cases} \tag{71}$$

where $C = 0$ if $r_{\rm in} > 0$ or $\ell > 0$. In these instances, the choice $B = \phi_w(r_w/r_{\rm UH})^{\ell}$ matches the boundary conditions at $r = r_w$, so the oscillation amplitude is clamped by the value at the wall. But, if $r_{\rm in} = 0$ and $\ell \le 0$ either B or C is undetermined, so any oscillation amplitude is allowed; these are singular upper hybrid eigenmodes. These modes make no potential outside the plasma; they are internal modes. Note that these occur only if there is no interior conductor ($r_{\rm in} = 0$). Finite temperature effects on these modes will be discussed in Secs. VII–IX.

B. Surface cyclotron waves for no inner conductor

Turning to the surface cyclotron waves, we first examine the case where there is no interior conductor. In this case, the solution domain includes $r = 0$, and then Eq. (66) implies that nontrivial solutions for $u(r)$ exist only for $\ell \ge 1$. These waves have angular phase velocity $\omega/\ell \sim \Omega_{c_s}/\ell$ in the same direction as the cyclotron motion. Then, Eq. (66) along with Eq. (69) implies that

$$\delta\phi(r) = Ar^{-\ell}\int_0^r dr' \frac{r'^{(2\ell-1)}}{D(r')}, \quad \ell > 0. \tag{72}$$

The constant A is determined by the boundary condition that $\delta\phi(r_w) = \delta\phi_w$,

$$A = \frac{r_w^{\ell}\delta\phi_w}{\int_0^{r_w} dr' r'^{(2\ell-1)}/D(r')}. \tag{73}$$

A dimensionless measure of the system response to the applied potential $\delta\phi_w$ is the admittance function Y, where

$$Y \equiv \frac{r_w \partial\delta\phi/\partial r_w}{\delta\phi_w}. \tag{74}$$

This function is proportional to the surface charge on the wall electrode for a given wall potential. The out-of-phase (imaginary) component of Y is due only to the plasma and is a useful measure of the amplitude of the plasma response to the applied wall potential. Using Eq. (51), the admittance can be expressed in terms of $\delta\phi_w$ and $u(r_w)$ as

$$\begin{aligned} Y &= -\ell + r_w\frac{u(r_w)}{\delta\phi_w}, \\ &= -\ell + \frac{r_w^{2\ell}}{\int_0^{r_w} dr' r'^{2\ell-1}/D(r')}. \end{aligned} \tag{75}$$

The imaginary part of the admittance has peaks at frequencies for which the denominator in Eq. (75) is small, i.e., where

$$\int_0^{r_w} dr'\, r'^{(2\ell-1)}/D(r') \to 0. \tag{76}$$

For finite collisional damping and real ω, this integral never equals zero, but for weak damping, minima in its magnitude approach zero at one or more frequencies corresponding to the frequencies of weakly damped cyclotron modes in the cold fluid limit. For the case of a uniform rotation frequency ω_E and a uniform density (possibly hollow) plasma column with outer radius r_2 and inner radius r_1 (similar to the species 2 profile shown in Fig. 1), the integral in Eq. (76) can be performed analytically. There is a single mode frequency for each (positive) value of ℓ, given by

$$\omega + i\nu - \Omega_{c_s} = (\ell-2)\omega_E + \beta\left(1 - \frac{r_2^{2\ell} - r_1^{2\ell}}{r_w^{2\ell}}\right), \quad \ell \geq 0. \tag{77}$$

The frequency shift $\ell\omega_E$ arises from the Doppler effect due to plasma rotation. The term $-2\omega_E$ arises from a shift in the cyclotron frequency caused by the Coriolis force. The term proportional to β is the frequency shift due to the self-consistent plasma electric field created by the perturbation. The shift is reduced by the factor $(r_2^{2\ell} - r_1^{2\ell})/r_w^{2\ell}$ due to the effect of image charge electric fields.

For more general density and rotation profiles, the integral in Eq. (76) must be performed numerically. In the limit of weak damping, $\nu \to 0$, there is a singularity in the integrand at radial locations $r_{\rm UH}$ where $D(r) \to 0$, corresponding to the aforementioned upper hybrid cutoff. If there is only one such location, at $r = r_{\rm UH}$, application of the Plemelj formula to Eq. (72) for $\nu \to 0^+$ allows one to write the admittance as

$$Y = -\ell + r_w^{2\ell} \Big/ \left[\mathcal{P}\int_0^{r_w} dr' \frac{r'^{(2\ell-1)}}{D(r')} - \frac{\pi i\, r_{\rm UH}^{2\ell-1}}{|D'(r_{\rm UH})|}\right]. \tag{78}$$

This expression shows that if the density or rotation frequency gradient is large (which makes $|D'|$ large), the amount of enhanced absorption due to the upper hybrid cutoff will be small. (This is why no effect of the cutoff appears in Eq. (77)–the cutoff occurs on the plasma edge, which was taken to be arbitrarily narrow.) An example with an edge of finite width is shown in Fig. 2. Here, we plot the imaginary part of Y versus the applied frequency for a single-species plasma with a density profile of the form

$$n(r) = \frac{n_0}{2}\left[\tanh\left(\frac{r_2 - r}{\Delta r}\right) + 1\right], \tag{79}$$

with associated equilibrium potential (and hence rotation frequency) given by the solution to Poisson's equation, $\nabla^2\phi_0 = -4\pi q^2 n(r)$. Here, and throughout the paper, we take $r_2 = r_w/2$. For this profile, there is a range of frequencies for which there is a single cutoff. For finite edge width Δr, even if $\nu \to 0$ the peak in Im Y has finite frequency width caused by energy absorption at the upper hybrid cutoff. The width in Im Y decreases as Δr decreases (Fig. 3). Also, as Δr decreases, the location of the peak in the plasma response approaches the analytic result given by Eq. (77), shown by the arrow in the figure.

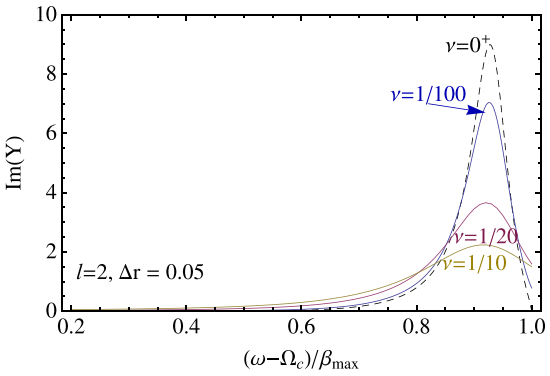

FIG. 2. Imaginary part of the admittance versus frequency for an $\ell = 2$ wall perturbation, in the cold fluid limit, at different collision frequencies ν (measured in units of $\beta_{\max} = \text{Max}\,(\beta)$ for the density profile of Eq. (79) with $r_2 = r_w/2, \Delta r = r_w/20$, where r_w is the wall radius).

We will see in Secs. VIII and IX that this absorption is due to the coupling of the surface cyclotron wave to Bernstein waves. The Bernstein waves draw energy from the surface cyclotron wave, causing a broadened frequency response. This damping mechanism is similar to the absorption of unmagnetized surface plasma wave energy that occurs at bulk plasma resonances in an inhomogeneous unmagnetized plasma.[19]

C. Surface cyclotron waves for an inner conductor with radius $r_{\rm in} > 0$

For the boundary conditions $\delta\phi(r_{\rm in}) = 0, \delta\phi(r_w) = \phi_w$, the origin is not in the solution domain and, therefore, Eq. (66) provides nontrivial surface cyclotron mode solutions for all integers ℓ. Now the perturbed potential is, from Eqs. (68) and (66),

$$\delta\phi(r) = Ar^{-\ell}\int_{r_{\rm in}}^{r_w} dr' \frac{r'^{(2\ell-1)}}{D(r')}, \tag{80}$$

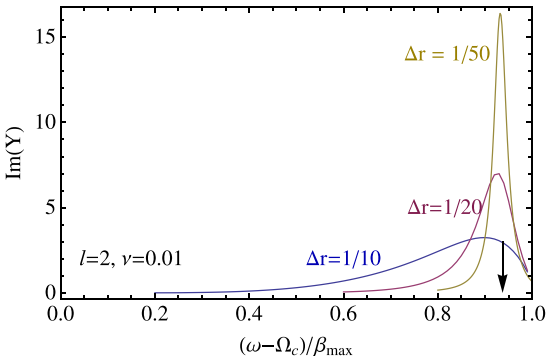

FIG. 3. Same as Fig. 2 but for fixed $\nu = \beta_{\max}/100$, at different profile widths Δr (in units of r_w). The arrow shows the frequency for a step profile, Eq. (77).

and the constant A is again given by the condition that $\delta\phi(r_w) = \phi_w$. The admittance is then given by Eq. (74)

$$Y = \frac{r_w^{2\ell}}{\int_{r_{\rm in}}^{r_w} dr' r'^{(2\ell-1)}/D(r')} - \ell. \tag{81}$$

Peaks in the admittance function again appear where the denominator approaches zero,

$$\int_{r_{\rm in}}^{r_w} dr' \frac{r'^{(2\ell-1)}}{D(r')} \to 0. \tag{82}$$

For example, for a uniform density hollow column with inner and outer radii r_1 and r_2 and with uniform rotation frequency ω_E, there is again one cyclotron mode per ℓ value, at frequency

$$\omega + i\nu - \Omega_{c_s} = (\ell - 2)\omega_E + \beta\left(1 - \frac{(r_2/r_w)^{2\ell} - (r_1/r_w)^{2\ell}}{1 - (r_{\rm in}/r_w)^{2\ell}}\right). \tag{83}$$

For $\ell > 0$ and $r_{\rm in} \to 0$, this formula returns to the previous result, Eq. (77). However, there are now also modes for $\ell \le 0$. For example, for $\ell = 0$, Eq. (83) reduces to

$$\omega + i\nu - \Omega_{c_s} = -2\omega_E + \beta\frac{\ln\left(\frac{r_w r_1}{r_{\rm in} r_2}\right)}{\ln(r_w/r_{\rm in})}, \quad \ell = 0. \tag{84}$$

This is the frequency of a cyclotron "breathing" mode, where the column oscillates radially without changing its density.

For more general density profiles with an inner conductor, for which Eq. (83) roughly applies, there are not necessarily any locations where $D(r) = 0$ in the plasma (unlike the previous example with no inner conductor), so in cold fluid theory, these modes are then undamped "discrete" eigenmodes when $\nu = 0$.

An example is shown in Fig. 4 for $\ell = 0$ and the same tanh density profile as we used for Figs. 2 and 3, taking $r_{\rm in} = r_1 = 1/10\, r_w$. The potential on the inner conductor is chosen so that ω_E is uniform inside the plasma far from the edges. Now, as ν decreases for any fixed value of Δr, peaks in Im Y become narrower without limit, signifying a discrete undamped mode in the $\nu \to 0$ limit. For small Δr, the peak in the plasma response occurs at the frequency predicted by Eq. (84) (the arrow in Fig. 4).

The modes are undamped as $\nu \to 0$ in this example because, for the range of frequencies plotted in Fig. 4, there is no longer an upper hybrid cutoff, although D changes sign from a negative value inside the plasma to a positive value (unity) outside it. This is because D changes sign by passing through infinity, since $\alpha(r) = 0$ at a location inside the plasma. This is the location of a wave-particle "resonance" that has important implications for finite-temperature cyclotron wave propagation.

Because the frequency of the surface cyclotron mode depends on species density, measurement of the mode frequency is a useful and nondestructive diagnostic for the density of each species.[2] The internal upper hybrid modes have frequencies given by Eq. (70), which also depend on density and rotation frequency, but these modes may be harder to detect experimentally. There are no peaks in the admittance function Y, indicating that, within the model of an infinitely long plasma column, these modes cannot be observed by their effect on wall image charges. On the other hand, it should be possible to detect these modes using a wall electrode located at the end of a finite-length plasma column.

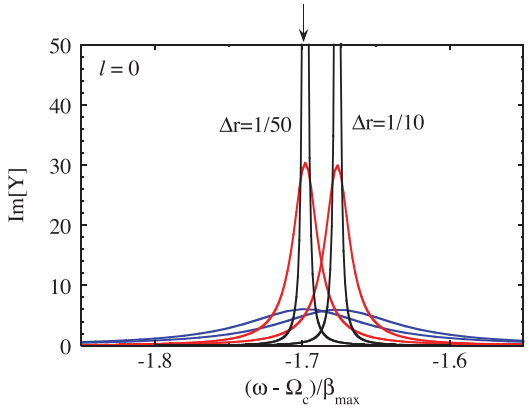

FIG. 4. Imaginary part of the admittance for an $\ell = 0$ cold-fluid cyclotron mode in a plasma with an inner conductor of radius $r_{\rm in} = r_w/10$, for two values of the profile width Δr (in units of r_w) and for $\nu/\beta_{\rm max} = 1/20$, 1/100 and 1/1000 (in order from broadest to sharpest admittance curves). The arrow shows the frequency for a step profile, Eq. (84).

VII. FINITE TEMPERATURE EFFECTS, BERNSTEIN WAVES

When finite temperature terms are added to the analysis of the surface cyclotron waves, new waves appear, referred to as Bernstein waves. These waves were analyzed qualitatively by Gould.[5,6] We will see that these waves couple to the surface cyclotron waves. Also, when there is no inner conductor, the $\ell \le 0$ singular upper hybrid continuum given by Eq. (70) breaks into another set of finite temperature Bernstein eigenmodes, which do not couple to the surface cyclotron waves.

The perturbed potential now satisfies

$$\nabla_\ell^2 \delta\phi + 4\pi q^2(\delta n_{F_s} + \delta n_{T_s}) = 0, \tag{85}$$

where δn_{F_s} and δn_{T_s} are given by Eqs. (50) and (55). For now, we consider only boundary conditions with no inner conductor where $r = 0$ is included in the domain, and $\delta\phi$ is specified on the outer wall. We also assume, for now, that the species s density profile extends to the origin, and that there is a vacuum region between the plasma and the wall.

Inside the plasma, Eq. (85) is a fourth order homogeneous equation for $\delta\phi$, or, alternately, a third order equation for u when we apply Eq. (61), but outside the equation reverts to Laplace's equation, second order in $\delta\phi$ (first order in u). The general solution of the third order equation for u is a sum of three independent solutions, $u_1(r), u_2(r), u_3(r)$.

For $\ell > 0$, it can be shown that one of these solutions (u_3, say) blows up at the origin. The interior solution within the plasma is then

$$u_{\rm in}(r) = B_1 u_1(r) + B_2 u_2(r). \tag{86}$$

This must be matched onto the outer Laplace solution at the plasma edge. The outer Laplace solution is

$$u_{\rm out} = A r^{\ell-1}. \tag{87}$$

The matching of inner and outer solutions is accomplished by setting

$$u_{\rm in}(r_{\rm out}) = u_{\rm out}(r_{\rm out}), \tag{88}$$

where $r_{\rm out}$ is a radius outside the plasma (typically chosen close to the plasma edge), where Eq. (85) is first-order. A WKB analysis (Sec. VIII) shows that only one of the two interior solutions remains finite outside the plasma (u_1, say); the other blows up as $n(r) \to 0$. Therefore, we set $B_2 = 0$, so Eqs. (86)–(88) determine B_1 in terms of A,

$$B_1 = A\, r_{\rm out}^{\ell-1}/u_1(r_{\rm out}). \tag{89}$$

Finally the constant A is determined in terms of the applied wall potential via Eq. (69),

$$\phi_w = B_1 r_w^{-\ell} \int_0^{r_{\rm out}} u_1(r) r^\ell dr + A r_w^{-\ell} \int_{r_{\rm out}}^{r_w} r^{2\ell-1} dr \tag{90}$$

(taking $C = 0$ since $\ell > 0$ is assumed).

Equation (90) determines the amplitude of the plasma response to the applied wall potential ϕ_w. This amplitude is unbounded wherever the rhs of Eq. (90) equals zero, i.e.,

$$0 = r_{\rm out}^{\ell-1} \int_0^{r_{\rm out}} u_1(r) r^\ell dr + u_1(r_{\rm out}) \int_{r_{\rm out}}^{r_w} r^{2\ell-1} dr. \tag{91}$$

These zeros correspond to a sequence of normal modes–the aforementioned Bernstein modes. The behavior of these modes is analyzed in the next sections.

For $\ell \le 0$, one can show that two of the three interior solutions blow up at the origin (u_2 and u_3, say), so

$$u_{\rm in}(r) = B_1 u_1(r). \tag{92}$$

This interior solution is not necessarily finite outside the plasma; it generally blows up as density $n_s \to 0$, so the only solution is $A = B_1 = 0$, i.e., $u = 0$. Then, Eq. (69) implies that the solution for $\delta\phi$ is a vacuum potential: $\delta\phi = \delta\phi_w (r/r_w)^{-\ell}$. However, there may be certain choices of ω for which the interior solution does not blow up. These frequencies correspond to eigenfrequencies of $\ell \le 0$ Bernstein oscillations.

In the cold-fluid theory, the $\ell \le 0$ upper hybrid oscillations were excited over a continuum of frequencies associated with an upper hybrid cutoff and were localized to a given radius for a given frequency in the continuum. With finite temperature, these modes are not localized and may occur only at discrete frequencies.

VIII. WKB ANALYSIS OF FINITE TEMPERATURE CYCLOTRON MODES

The previous general ideas concerning the solution of Eq. (85) can be illustrated and expanded using a WKB solution of the problem. We first make some general observations about the Bernstein wave solutions expected from this analysis. For a uniform plasma in the low-density regime $\omega_p/\Omega_c \ll 1$, the finite-T dielectric constant $D_T(\omega, k)$ near the cyclotron frequency for species s is[18,20]

$$D_T(\omega, k) = 1 - \frac{2\beta\Omega_{c_s}}{\omega(\omega - \Omega_{c_s})} e^{-k^2 r_c^2} \frac{I_1(k^2 r_c^2)}{k^2 r_c^2}, \tag{93}$$

where $I_1(x)$ is a modified Bessel function. The zeros of the dielectric constant yield the Bernstein mode dispersion relation,

$$\begin{aligned}\omega(k) &= \Omega_{c_s} + 2\beta\, e^{-k^2 r_c^2} \frac{I_1(k^2 r_c^2)}{k^2 r_c^2} + O\left(\frac{1}{\Omega_c^2}\right) \\ &= \Omega_{c_s} + \beta(1 - k^2 r_c^2 + \ldots), \quad k r_c \ll 1.\end{aligned} \tag{94}$$

The time-averaged energy density in the waves is

$$E_w = \frac{|\mathbf{E}|^2}{16\pi} \frac{\partial}{\partial\omega}(\omega D_T) = \frac{|\mathbf{E}|^2}{16\pi} \frac{\Omega_c}{\omega - \Omega_c}, \tag{95}$$

where $\mathbf{E} = -\nabla\delta\phi$ is the wave electric field. The energy flux is

$$\mathbf{S} = \mathbf{v}_g E_w, \tag{96}$$

and

$$\mathbf{v}_g = \frac{\partial\omega}{\partial\mathbf{k}} = -4\beta r_c \frac{[k^2 r_c^2 (I_1 - I_0) + 2I_1]}{k^3 r_c^3} e^{-k^2 r_c^2} \hat{k} \tag{97}$$

is the group velocity.

Our wave Eq. (85) should produce results consistent with the small k limit of these expressions. Outside the plasma, the solution for $u(r)$ is given by Eq. (87). Inside, we assume a WKB form

$$u(r) = e^{S(r)}, \tag{98}$$

where we expand the eikonal $S(r)$ in a power series in the cyclotron radius r_c,

$$S(r) = \frac{S_0(r)}{r_c} + S_1(r) + r_c S_2(r) + \cdots. \tag{99}$$

This asymptotic expansion will be useful provided that $r_c/\mathcal{L} \ll 1$, where $\mathcal{L}$ is the scale length of the equilibrium. The only term in $\delta n_T(r)$ that enters the analysis to determine S_0 and S_1 is the first term in Eq. (56).

Substituting Eqs. (98) and (99) into Eq. (85) and keeping the lowest order terms in r_c yields the following equation for S_0:

$$D\,S_0' - \frac{\beta}{\alpha} S_0'^3 = 0. \tag{100}$$

This implies $S_0' = 0$ or $S_0' = \pm ik(r) r_c$, where

$$k(r) \equiv \sqrt{-\alpha D/(\beta r_c^2)} = \sqrt{1-\alpha/\beta}\,/r_c \tag{101}$$

is the local radial wavenumber of the solution. For the case $S_0' = 0$, the solution is slowly varying and is entirely determined at the next order.

Considering the next-order equation in r_c yields the following expression for S_1 when $S_0' = 0$:

$$S_1' + \frac{D'}{D} - \frac{(\ell-1)}{r} = 0. \tag{102}$$

The solution is the cold fluid result $S_1 = -\log D + (\ell-1)\log r$, or

$$u_1(r) = \frac{r^{\ell-1}}{D(r)}. \tag{103}$$

An order r_c^2 correction to this solution could be found by working to even higher order, but we will not use that correction here. This cold fluid solution is invalid if $1/D(r)$ varies rapidly, which occurs near the upper hybrid cutoff where $D(r) = 0$.

The amplitudes of the other two rapidly varying solutions with $S_0' = \pm ik(r) r_c$ are also obtained by considering the next-order equation in r_c, which now yields

$$S_1'(r) + \frac{1}{2r} + \frac{1}{r}\left(\frac{D'}{D} + \frac{\beta'}{\beta} - \frac{\alpha'}{\alpha}\right) = 0. \tag{104}$$

Thus, the second and third WKB solutions for $u(r)$ are

$$u_{2,3}(r) = \frac{1}{\sqrt{r}}\left(\frac{\alpha}{\beta D}\right)^{\frac{1}{4}} e^{\pm i\int^r k(r)dr}. \tag{105}$$

These solutions are traveling waves moving radially inward or outward, depending on the sign of ω and Re(k). Their wavenumber and amplitude (but not their frequency) vary in radius as the plasma density and/or rotation rate varies. The local dispersion relation of these waves follows from Eq. (101):

$$\alpha = \beta(1 - k^2 r_c^2). \tag{106}$$

Equation (106) matches the long-wavelength limit of the Bernstein-mode dispersion relation, Eq. (94), for the shear-free case; noting that for a rotating system, there is a Doppler shift to ω and a shift to Ω_c from the Coriolis force that appears in Eq. (106) through α [see Eq. (53)]. The radial group velocity follows from the derivative with respect to k of Eq. (106):

$$\mathrm{v}_g = -2\beta k r_c^2. \tag{107}$$

The WKB amplitude factor for the Bernstein waves,

$$u \propto \frac{1}{\sqrt{r}}\left(\frac{\alpha}{\beta D}\right)^{1/4}, \tag{108}$$

is consistent with energy conservation. For WKB traveling waves, the conserved quantity is the total radial energy flux $r\mathbf{S}\cdot\hat{r}$ given by Eq. (96). Identifying $\omega - \Omega_c$ with α and identifying $|\mathbf{E}|^2$ with u^2 [using Eq. (52) and the WKB limit $kr \gg \ell$] implies the following general WKB amplitude factor:

$$u \propto \left(-\frac{\alpha(r)}{r\Omega_{c_s}\mathrm{v}_g(r,k)}\right)^{1/2}. \tag{109}$$

To compare this to Eq. (108), we substitute for v_g from Eq. (107), noting that the group velocity can be written as $\mathrm{v}_g = -2\beta r_c\sqrt{1-\alpha/\beta}$ using Eq. (106). Substituting this expression into Eq. (109) and using Eq. (52) yields Eq. (108), the $kr_c \ll 1$ form of the amplitude factor.

The two WKB solutions in Eq. (105) break down near $r = 0$; near any upper hybrid cutoffs where $D(r) \to 0$; and near any "resonances" where $\alpha(r) = 0$ and $D(r) \to \infty$, corresponding to strong wave-particle resonant interactions. These resonances, if they occur, cause damping of Bernstein waves. Note that the slowly varying "cold fluid" solution u_1 also breaks down at the upper hybrid cutoff, but not at $r = 0$ or at the $\alpha = 0$ resonance. Also, when $\beta(r) \to 0$ at the plasma edge, Eq. (101) implies that $k \to i\infty$, so one Bernstein solution blows up and the other decays to zero exponentially.

Connection formulae[18] must be derived in order to connect WKB solutions on either side of a cutoff or resonance. We first consider the connection formula for a cutoff.

A. Connection formula for an upper hybrid cutoff

Consider a situation where $Re(\alpha(r)) > 0$ but $Re(D(r))$ changes sign at $r = r_{\mathrm{UH}}$, with $Re(D) > 0$ for $r > r_{\mathrm{UH}}$ (see Fig. 5). Near $r = r_{\mathrm{UH}}$, $D(r) \simeq (r - r_{\mathrm{UH}})/\mathcal{L}$, where $\mathcal{L}^{-1} \equiv D'(r_{\mathrm{UH}}) > 0$ by assumption. On the left side of the cutoff, we write the WKB solution as

$$u_L(r) = \frac{A_L r^{\ell-1}}{D(r)} + \frac{B_L}{\sqrt{r}}\left(\frac{-\alpha}{\beta D}\right)^{\frac{1}{4}}\cos\left[\int_{r_{\mathrm{UH}}}^{r} k dr + \chi\right], \tag{110}$$

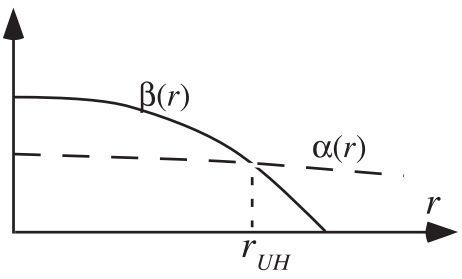

FIG. 5. Schematic of a plasma for which there is a single upper hybrid cutoff. Varying ω moves the $\alpha(r)$ profile vertically and changes the location of the cutoff.

where A_L and B_L are the amplitudes of the solution and χ is the phase. [Throughout the remainder of the paper, we assume a sign in the square root in Eq. (101) such that $\mathrm{Re}\, k > 0$. In this section, we use the $kr_c \ll 1$ form of the WKB amplitude factor, Eq. (108), since near cutoff $k \to 0$.] On the right side of the cutoff, the WKB solution is

$$u_R(r) = \frac{A_R r^{\ell-1}}{D(r)} + \frac{1}{\sqrt{r}}\left(\frac{\alpha}{\beta D}\right)^{\frac{1}{4}}\left[B_{R_1} e^{\int_{r_{\mathrm{UH}}}^{r} kdr} + B_{R_2} e^{-\int_{r_{\mathrm{UH}}}^{r} kdr}\right]. \tag{111}$$

To connect these two solutions, we note that near $r = r_{\mathrm{UH}}$, Eq. (85) can be approximated as

$$-r_c^2\, u'''(x) + \frac{\partial}{\partial x}\left(\frac{x}{\mathcal{L}}\, u\right) = 0, \tag{112}$$

where $x = r - r_{\mathrm{UH}}$, we have used the relation $\beta/\alpha|_{r=r_{\mathrm{UH}}} = 1$, and we have kept only the dominant balance in Eq. (85), assuming $r_c/\mathcal{L} \ll 1$. [This balance involves only the first term in δn_F (see Eq. (50)) and the first term in Eq. (56).] The general solution can be written in terms of Airy functions and integrals of Airy functions:

$$u(x) = D_1 A_i(\bar{x}) + D_2 B_i(\bar{x}) + D_3 C_i(\bar{x}), \tag{113}$$

where the function C_i is defined as

$$C_i(\bar{x}) \equiv \pi A_i(\bar{x}) \int_{-\infty}^{\bar{x}} dx_0 B_i(x_0) + \pi B_i(\bar{x}) \int_{\bar{x}}^{\infty} dx_0 A_i(x_0) \tag{114}$$

and $\bar{x} \equiv x/(\mathcal{L} r_c^2)^{1/3}$. For $\bar{x} \ll -1$ but $|x|/\mathcal{L} \ll 1$, we can connect Eq. (110) to Eq. (113) using the asymptotic form of Eq. (113). The asymptotic forms of the Airy functions A_i and B_i are well known.[21] The asymptotic forms for $C_i(\bar{x})$ are

$$\begin{aligned} C_i(\bar{x}) &= \frac{1}{\bar{x}} + \frac{2}{\bar{x}^4} + \frac{40}{\bar{x}^7} + \cdots + \frac{\sqrt{\pi}}{(-\bar{x})^{1/4}} \cos\left[\frac{2}{3}(-\bar{x})^{3/2} + \frac{\pi}{4}\right] \\ &\quad \times \left(1 + \frac{385}{4608\bar{x}^3}\cdots\right) + \frac{5}{48}\frac{\sqrt{\pi}}{(-\bar{x})^{7/4}} \sin\left[\frac{2}{3}(-\bar{x})^{3/2} + \frac{\pi}{4}\right] \\ &\quad \times \left(1 + \frac{17017}{13824\bar{x}^3} + \cdots\right), \quad \bar{x} \ll -1 \\ C_i(\bar{x}) &= \frac{1}{\bar{x}} + \frac{2}{\bar{x}^4} + \frac{40}{\bar{x}^7}\ldots, \quad \bar{x} \gg 1. \end{aligned} \tag{115}$$

Using the $\bar{x} \ll -1$ asymptotic form in Eq. (113) along with the corresponding forms for the Airy functions yields the following lowest-order form for u:

$$\lim_{\bar{x}\to-\infty} u(x) = \frac{1}{\sqrt{\pi}(-\bar{x})^{1/4}}\left[D_1 \sin\left(\frac{2}{3}(-\bar{x})^{3/2} + \frac{\pi}{4}\right) + (D_2 + \pi D_3)\cos\left(\frac{2}{3}(-\bar{x})^{3/2} + \frac{\pi}{4}\right)\right] + \frac{D_3}{\bar{x}}. \tag{116}$$

Comparing Eq. (116) to Eq. (110), and noting that for $0 \le (r_{\mathrm{UH}} - r)/\mathcal{L} \ll 1$, we can approximate $\frac{2}{3}|\bar{x}|^{3/2} = \int_r^{r_{\mathrm{UH}}} kdr$, $D(r) = x/\mathcal{L}$, and $(-\alpha/(\beta D))^{1/4} = (-\mathcal{L}/x)^{1/4}$, so we obtain

$$A_L = D_3 r_{\mathrm{UH}}^{1-\ell}(r_c^2/\mathcal{L}^2)^{1/3}, \tag{117}$$

$$B_L \cos\chi = \sqrt{\frac{r_{\mathrm{UH}}}{2\pi}}(r_c/\mathcal{L})^{1/6}[D_1 + D_2 + \pi D_3], \tag{118}$$

$$B_L \sin\chi = \sqrt{\frac{r_{\mathrm{UH}}}{2\pi}}(r_c/\mathcal{L})^{1/6}[D_1 - D_2 - \pi D_3]. \tag{119}$$

On the right side of the cutoff the lowest order asymptotic form of Eq. (113) is

$$\lim_{\bar{x}\to\infty} u(x) = \frac{1}{\sqrt{\pi}\,\bar{x}^{1/4}}\left[\frac{1}{2} e^{-2\bar{x}^{3/2}/3} D_1 + D_2 e^{2\bar{x}^{3/2}/3}\right] + D_3/\bar{x}. \tag{120}$$

Connecting to Eq. (111) for $\bar{x} \gg 1$ but $(r - r_{\mathrm{UH}})/\mathcal{L} \ll 1$ implies

$$A_R = D_3 r_{\mathrm{UH}}^{1-\ell}(r_c/\mathcal{L})^{2/3}, \tag{121}$$

$$B_{R_1} = \sqrt{\frac{r_{\mathrm{UH}}}{\pi}}(r_c/\mathcal{L})^{1/6} D_2, \tag{122}$$

$$B_{R_2} = \sqrt{\frac{r_{\mathrm{UH}}}{\pi}}(r_c/\mathcal{L})^{1/6}\frac{D_1}{2}. \tag{123}$$

Eliminating D_1, D_2, and D_3 from Eqs. (117)–(119) and (121)–(123) yields the connection formulae at an upper hybrid cutoff,

$$A_L = A_R, \tag{124}$$

$$B_L \cos\chi = \frac{B_{R_1}}{\sqrt{2}} + \sqrt{2} B_{R_2} + \sqrt{\frac{\pi\mathcal{L}}{2r_c}} r_{\mathrm{UH}}^{\ell-1/2} A_R, \tag{125}$$

$$B_L \sin\chi = -\frac{B_{R_1}}{\sqrt{2}} + \sqrt{2} B_{R_2} - \sqrt{\frac{\pi\mathcal{L}}{2r_c}} r_{\mathrm{UH}}^{\ell-1/2} A_R. \tag{126}$$

These formulae indicate that, at a cutoff, the slowly varying "cold fluid" solution, responsible for surface cyclotron waves, and proportional to coefficients A_R and A_L, is mixed with the rapidly varying "Bernstein" solutions, proportional to B_R and B_L.

B. Behavior near a resonance

There may be locations in the plasma where $\alpha(r) = 0$, due to shears in the $E \times B$ rotation frequency. At such locations, the WKB Bernstein mode solutions, Eq. (105), are invalid. This is because Eq. (101) implies that $kr_c = 1$ at $\alpha = 0$, which breaks the assumption used to derive Eq. (85) that $kr_c \ll 1$. Therefore, we modify the Bernstein WKB solutions by using the exact Bernstein mode dispersion relation for a uniform system, Eq. (94), writing the dispersion relation as

$$\alpha(r) = 2\beta(r)\, e^{-k^2 r_c^2}\, \frac{I_1(k^2 r_c^2)}{k^2 r_c^2} \tag{127}$$

in order to account for Doppler and Coriolis force shifts due to plasma rotation. This WKB dispersion relation agrees

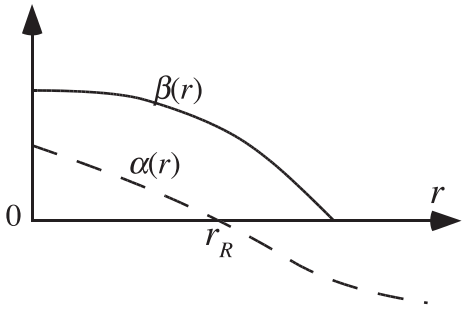

FIG. 6. Schematic of a plasma with parameters chosen so that there is a single resonance.

with the $\omega_p/\Omega_c \ll 1$ limit of the Bernstein dispersion relation for a rotating uniform density single species plasma column, derived in Ref. 22. This equation shows that at a resonance, the radial wavenumber k approaches infinity, not $1/r_c$ as our approximate dispersion relation, Eq. (106), predicted.

Furthermore, the resonance does not act as a turning point for rays, unlike the upper hybrid cutoff. The rays are curves in the (r, k_r) plane describing the trajectory of Bernstein wave packets. The rays are obtained from Eq. (127), as contours of constant ω.[23] When $\alpha(r)$ and $\beta(r)$ have the form shown in Fig. 6, these constant ω contours have the form shown schematically in Fig. 7(a). The rays are simply diverted to large k without reflecting, as opposed to the case of a upper hybrid cutoff (Fig. 5), for which the rays have a turning point (Fig. 7(b)).

Furthermore, the WKB wave amplitude becomes large at the resonance. As $kr_c \to \infty$, Eq. (127) implies that

$$\alpha(r) \to \sqrt{\frac{2}{\pi}}\,\frac{\beta(r)}{k^3 r_c^3}, \tag{128}$$

so the radial group velocity approaches zero as

$$\mathrm{v}_g \to -3\sqrt{\frac{2}{\pi}}\,\frac{\beta(r)}{k^4 r_c^3}. \tag{129}$$

Using these equations in the expression for conservation of energy flux, Eq. (96) implies that, near the resonance where $\alpha \to 0$,

$$|\mathbf{E}|^2 \propto \frac{1}{[\alpha(r)]^{1/3}}. \tag{130}$$

These large amplitude large k Bernstein waves will be absorbed by the plasma at the resonance. The absorption mechanism could be viscous damping due to large k, nonlinear processes due to large amplitude such as wave-breaking, or direct Landau damping at the resonance. [None of these effects are included in Eq. (85), which does not apply at a resonance.] Such damping is observed in experiments on fusion plasmas.[10]

Since the Bernstein waves are absorbed at a resonance rather than being reflected, there are generally no longer any Bernstein normal modes in WKB theory, since normal modes are standing waves that require interference between waves propagating radially in both directions. However, a reflection is still possible if there is an abrupt density change in the plasma with $k\mathcal{L} < 1$, which violates the WKB approximation. This case has been considered by Spencer *et al.* for $\ell = 0$ modes.[24]

On the other hand, the cold fluid solution to Eq. (85) passes through the resonance, essentially unchanged. In cold fluid theory, we have already observed that the solution for $u(r)$, Eq. (66), merely changes sign at locations where $\alpha(r) = 0$. When finite temperature corrections are added, we find that this is still the case provided that $r_c/\mathcal{L} \ll 1$. To derive this result, we expand $\alpha(r)$ near the resonance, writing

$$\alpha = \frac{\omega_0}{r_R}(r - r_R), \tag{131}$$

where

$$\omega_0 \equiv r_R \left.\frac{\partial \alpha}{\partial r}\right|_{r=r_R}. \tag{132}$$

Defining $f \equiv (\omega_0/r_R)u/\alpha$ and $x \equiv r - r_R$, so that $u = xf$, the dominant balance for $|x/r_R| \ll 1$ and $r_c/|r_R| \ll 1$ in Eq. (85) is

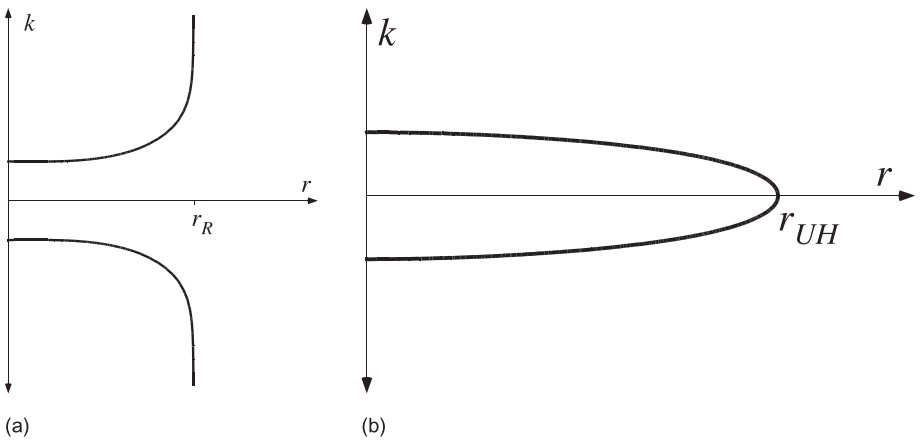

FIG. 7. (a) Rays (contours of constant ω) for Bernstein waves at a frequency corresponding to the $\alpha(r)$ profile in Fig. 6. (b) Analogous ray (contour of constant ω) for Bernstein waves at a frequency corresponding to the $\alpha(r)$ profile in Fig. 5.

$$r_c^2\left(f''' + \frac{\partial}{\partial x}\left(\frac{f'}{x}\right)\right) + f' = 0. \tag{133}$$

[This dominant balance involves the first term in Eqs. (50), (56), and (58), and Eq. (59).] The solution is

$$f = D_1 J_0\left(\frac{x}{r_c}\right) + D_2 Y_0\left(\frac{x}{r_c}\right) + D_3. \tag{134}$$

The Bessel functions J_0 and Y_0 are the two Bernstein wave solutions near resonance, but with an incorrect (finite) wavelength due to the aforementioned breakdown of Eq. (85) as kr_c becomes of order unity. However, the fluid solution to Eq. (85) remains valid provided that it remains slowly varying. In fact, for small r_c, Eq. (134) shows this to be true: near resonance the fluid solution for f is simply the constant D_3, which implies that $u = D_3\,\alpha(r)$. This solution can be asymptotically matched onto the fluid solution away from the resonance, Eq. (66), via the choice $D_3 = -Ar_R^{\ell-1}/\beta(r_R)$.

Thus, the fluid solution is unaffected by the resonance even when finite temperature effects are included (provided that r_c is small). This is illustrated in Fig. 8, which displays a solution of Eq. (85) for a single-species plasma with the density profile of Eq. (79) and for $\ell = 0$. For this ℓ value, there is a range of frequencies for which a single resonance occurs. The figure shows $u(r)$ for one such frequency and for $r_c = r_w/100$, compared to the fluid solution; the two solutions are matched at $r = 0.6r_w$. A small collision frequency ν is added to the frequency in order to regularize the poles in Eq. (85) that occur at the resonance; but the results displayed are in the limit of small ν. One can see that for small but finite r_c, the fluid solution closely follows the numerical solution.

IX. WKB SOLUTIONS: EXAMPLES

The connection formulae derived in Sec. VIII B can be used to solve for the potential response of a finite-temperature plasma to an oscillatory wall signal. The behavior of the solutions is influenced by the locations of cutoffs and resonances. We consider several examples.

A. One upper-hybrid cutoff

The simplest example is the case of a single upper-hybrid cutoff. For instance, this can occur for the lightest species in a multi-component plasma with nearly uniform total density that has undergone some centrifugal separation; see Fig. 1.[25] In this case, $\alpha(r)$ is nearly constant over the range of radii for which $\beta(r)$ is nonzero, and there is a range of mode frequencies for which

$$0 < \alpha < \mathrm{Max}\,(\beta). \tag{135}$$

There is then a single cutoff at the radial location r_{UH} where $\alpha(r_{\mathrm{UH}}) = \beta(r_{\mathrm{UH}})$ (see Fig. 5). For frequencies outside this range, the real part of the dielectric constant $D(r)$ does not change sign and the plasma response is well-represented by the fluid limit, Eq. (66). This fluid response was already discussed in Sec. V.

For frequencies within the range given by Eq. (135), the upper hybrid cutoff causes reflection of the Bernstein waves that sets up a strong resonant plasma response at a discrete set of mode frequencies. Inside the plasma, to the left of the cutoff, $D(r) < 0$ and $\alpha > 0$, so the WKB solution for $u(r)$ is of the form given by Eq. (110)

$$u = \frac{A_L r^{\ell-1}}{D(r)} + B_L\left(-\frac{2r_c\alpha}{r v_g(r,k)}\right)^{1/2} \times \cos\left(\int_{r_{\mathrm{UH}}}^{r} k(r)dr + \chi\right), \quad r < r_{\mathrm{UH}}. \tag{136}$$

Here, we have used the general form for the WKB amplitude factor, Eq. (109), normalized so as to approach the $kr_c \ll 1$ form, Eq. (108), as kr_c becomes small. The phase χ is determined by the $r < r_{\mathrm{UH}}$ form of the solution near $r = 0$. For $r/\Delta r \ll 1$, we can take $n(r) \approx n_0$ and then the solution of Eq. (85) that is finite at $r = 0$ is

$$u(r) = \frac{A_L r^{\ell-1}}{D(r)} + E J_{\ell-1}(k_0 r), \quad \frac{r}{\mathcal{L}} \ll 1, \tag{137}$$

where $k_0 = k(0)$, and $J_\ell(x)$ is a Bessel function. This solution can be connected to Eq. (136) for $r/r_c \gg 1$ using the large argument form of the Bessel function.[21] This implies

$$\chi = \int_0^{r_{\mathrm{UH}}} k(r)dr - (\ell - 1)\frac{\pi}{2} - \frac{\pi}{4}. \tag{138}$$

To complete the solution for u, we match Eq. (136) to the form for $r > r_{\mathrm{UH}}$, using Eqs. (124)–(126) adding the requirements that the solution remain finite as $n(r) \to 0$, and the outer solution match to Eq. (87). This implies that the coefficient B_{R1} must vanish, so the matching conditions are

$$A_L = A, \tag{139}$$

$$B_L \cos\chi = \sqrt{2}\,B_{R2} + \sqrt{\frac{\pi\mathcal{L}}{2r_c}}\,r_{\mathrm{UH}}^{-1/2} A, \tag{140}$$

$$B_L \sin\chi = \sqrt{2}\,B_{R2} - \sqrt{\frac{\pi\mathcal{L}}{2r_c}}\,r_{\mathrm{UH}}^{-1/2} A, \tag{141}$$

where $\mathcal{L}^{-1} = D'(r_{\mathrm{UH}})$.

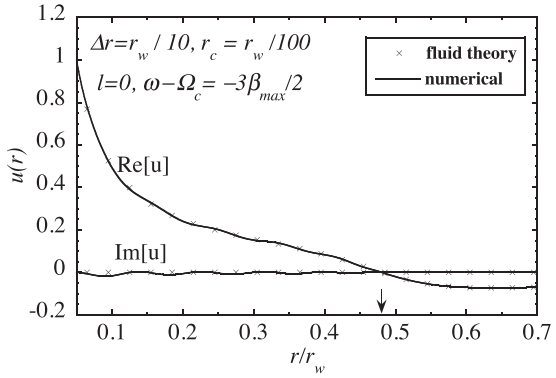

FIG. 8. Comparison of cold fluid theory, Eq. (66), to a solution to Eq. (85) when there is a resonance. Fluid solution and numerical solution are matched at $r/r_w = 0.6$. The resonance is located at the arrow.

Equations (140) and (141) can be used to determine B_{R2} and B_L in terms of A

$$B_L = \sqrt{\frac{\pi\mathcal{L}}{r_c}}\frac{r_{\rm UH}^{\ell-1/2}}{\cos(\chi+\pi/4)}A, \tag{142}$$

$$B_{R2} = \sqrt{\frac{\pi\mathcal{L}}{r_c}}\frac{r_{\rm UH}^{\ell-1/2}}{2}\tan\left(\chi+\frac{\pi}{4}\right)L. \tag{143}$$

Equation (69) then allows determination of the perturbed potential $\delta\phi$. Near $r=0$, substitution of Eq. (137) into Eq. (69) yields

$$\delta\phi(r) = Cr^{-\ell} + Ar^{-\ell}\int_0^r dr'\frac{r'^{2\ell-1}}{D(r')} + \frac{E}{k_0}J_\ell(k_0 r), \quad \frac{r}{\mathcal{L}} \ll 1, \tag{144}$$

where we require $C=0$ for $\ell>0$ and $A=0$ for $\ell\le 0$. This can be connected onto the WKB form by using the following integration identity, obtained using integration by parts:

$$\lim_{r_c\to 0}\int_a^b dr\, g(r)\, e^{i\Phi(r)/r_c} \simeq \frac{r_c}{i\Phi'(r)}g(r)\, e^{i\Phi(r)/r_c}\Big|_a^b + O(r_c^2), \tag{145}$$

provided that there are no locations in $a\le r\le b$, where $\Phi'(r)=0$. We break Eq. (69) into two terms,

$$\delta\phi = \delta\phi(Nr_c) + r^{-\ell}\int_{Nr_c}^r dr'\, r'^\ell u(r'), \tag{146}$$

where $N\gg 1$ but $Nr_c \ll \Delta r$. This allows use of the WKB form, Eq. (136) in the integral, and Eq. (144) in the first term. After asymptotic-expansion of J_ℓ for large argument, and cancellation of terms involving N, we obtain

$$\delta\phi(r) = Cr^{-\ell} + Ar^{-\ell}\int_0^r dr'\frac{r'^{2\ell-1}}{D(r')} + \frac{B_L}{k}\left(-\frac{2r_c\alpha}{r\mathrm{v}_g(k,r)}\right)^{1/2} \times \sin\left(\int_{r_{\rm UH}}^r k(r)dr + \chi\right), \quad r_c \ll r < r_{\rm UH}. \tag{147}$$

This form for $\delta\phi$ is valid to the left of the upper hybrid cutoff, but away from the origin.

To find $\delta\phi$ to the right of the cutoff, one must integrate across the cutoff using the connecting form, Eq. (113). We write Eq. (69) as

$$\delta\phi(r) = \delta\phi(r_{\rm UH}-Na_0) + r^{-\ell}\int_{r_{\rm UH}-Na_0}^{r_{\rm UH}+Na_0} dr'\, r'^\ell u(r') + r^{-\ell}\int_{r_{\rm UH}+Na_0}^r dr' r'^\ell u(r'), \tag{148}$$

where $a_0 \equiv (\mathcal{L}r_c^2)^{1/3}, N\gg 1$ but $N\,a_0/\mathcal{L}\ll 1$.

We can use the WKB form for $\delta\phi$, Eq. (147), in the first term. In the last term, we can use $u = Ar^{\ell-1}/D$, and in the middle term, we can use Eq. (113). Noting that $D(r) \simeq \mathcal{L}^{-1}(r-r_{\rm UH})$ for r near $r_{\rm UH}$, and using Eq. (107) for v_g near the cutoff where $kr_c\to 0$, Eq. (142) for B_L, Eqs. (139) and (117)–(119), we find that terms involving N cancel, and we are left with

$$\delta\phi(r) = Cr^{-\ell} + Ar^{-\ell}\mathrm{P}\!\!\!\!\!\!\int_0^r dr'\frac{r'^{(2\ell-1)}}{D(r')} + D_1 a_0 r_{\rm UH}^\ell r^{-\ell}, \tag{149}$$

where $\mathrm{P}\!\!\!\!\!\int$ means the principal part of the integral, neglecting the pole at $r=r_{\rm UH}$. In deriving Eq. (149), we have also used the identities $\int_{-\infty}^{\infty}A_i(\bar{x})\,d\bar{x}=1$ and $\lim_{N\to\infty}\int_{-N}^{N}C_i(\bar{x})\,d\bar{x}=0$. The latter follows by applying $\int_{-\infty}^{\infty}d\bar{x}$ to Eq. (114) and integrating by parts.

Substituting for D_1 from the solution of Eqs. (118)–(119) and using Eq. (142) yields

$$r^\ell\delta\phi(r) = C + A\left[\mathrm{P}\!\!\!\!\!\int_0^r dr'\frac{r'^{(2\ell-1)}}{D(r')} + \pi\mathcal{L}r_{\rm UH}^{2\ell-1}\tan\left(\chi+\frac{\pi}{4}\right)\right], \quad r-r_{\rm UH}\gg a_0. \tag{150}$$

For $\ell>0$, $C=0$ is required, so Eqs. (150), (75), and (51) determine the admittance

$$Y = \frac{r_w^{2\ell}}{\mathrm{P}\!\!\!\!\!\int_0^{r_w} dr' r'^{(2\ell-1)}/D(r') + \pi\mathcal{L}r_{\rm UH}^{2\ell-1}\tan[\chi+\pi/4]} - \ell. \tag{151}$$

Here, χ is given by Eq. (138), and k by Eq. (101) when α/β is close to unity (so that $kr_c\ll 1$). More generally, we can extend the validity of Eq. (151) to all kr_c by using Eq. (127) for k.

The first term in the denominator of Eq. (151) is the same as for cold fluid theory, Eq. (78). The second term leads to the Bernstein modes. These modes occur wherever the denominator vanishes, i.e., where

$$\int_0^{r_{\rm UH}} k dr = \frac{(\ell-1)\pi}{2} + n\pi - \arctan\left[\frac{r_{\rm UH}^{1-2\ell}}{\pi\mathcal{L}}\mathrm{P}\!\!\!\!\!\int_0^{r_w} dr'\frac{r'^{(2\ell-1)}}{D(r')}\right] \tag{152}$$

for any integer n [using Eq. (138)]. This is the dispersion relation for the $\ell>0$ Bernstein modes in the WKB limit for a single cutoff.

For a uniform density step profile of radius r_2 and assuming $kr_c\ll 1$, we can estimate the frequency predicted by Eq. (152) by taking k constant, given by Eq. (101), and $r_{\rm UH}\simeq r_2$, yielding

$$\alpha \simeq \beta\left(1-\frac{r_c^2}{r_2^2}x_n^2\right), \tag{153}$$

where x_n is the right hand side of Eq. (152). Note that in a step profile, $\mathcal{L}\to 0$ and $\arctan(\infty)=\pi/2$, so $x_n = (\ell/2\ +n)\pi$.

As mode number n increases, the frequency decreases, with a frequency spacing between modes proportional to plasma temperature through the factor r_c^2/r_2^2. (This result is only an estimate since a step profile has rapid variation that violates the WKB approximation $k\mathcal{L} \gg 1$. However, a solution of Eq. (85) for a step profile does predict Bernstein mode frequencies of the form given in Eq. (153), albeit with a different value for x_n.)

In Fig. 9, we display the admittance Y for the density profile given by Eq. (79), versus cyclotron radius r_c. The singularities of Y locate the frequencies of the Bernstein modes. We assume $\alpha(r)$ is uniform and equal to $4\,\mathrm{Max}\,(\beta)/5$, and for $\Delta r = r_w/10$, $r_2 = r_w/2$, and $\ell = 2$ using Eq. (101) for k. Equation (101) is correct only for small kr_c. We use this form for k in order to compare to numerical solutions of Eq. (85) (the dots in Fig. 6), which are valid only for $kr_c \ll 1$. The WKB form for this function, Eq. (151), is an excellent fit to the numerical solution of Eq. (85).

In Fig. 10, we show two of the potential eigenfunctions for these modes, compared to the WKB forms, using the $kr_c \ll 1$ expressions for the WKB wave number and amplitude in order to better compare to solutions of Eq. (85).

When there is finite damping ν, the admittance exhibits a sequence of peaks at frequencies determined by the solution of Eq. (152) (see Fig. 11, plotted for $\ell = 1$). In this figure, we use the general form for k, from a solution of Eq. (127) for $k(\alpha/\beta)$, rather than Eq. (101). The solution of Eq. (85) is compared to the WKB prediction on the right side of the figure, where $kr_c \ll 1$ for the Bernstein modes. The numerical solution differs from the WKB solution as $\alpha/\beta_{\max} \to 1$ because WKB theory breaks down as $k\mathcal{L}$ becomes small. For sufficiently small r_c, there is a regime for which both $kr_c \ll 1$ and $k\mathcal{L} \gg 1$, where the WKB and numerical solutions of Eq. (85) match.

As the cyclotron radius r_c decreases, the spacing between the admittance peaks in Fig. 11, and the height of the peaks, decreases until the result is indistinguishable from the cold-fluid admittance given by Eq. (78). This happens because, in Eq. (138), the imaginary part of χ (due to finite ν) becomes large and negative as r_c decreases, so that $\tan(\chi + \pi/4) \to -i$, implying that Eq. (151) becomes identical to Eq. (78). This will occur roughly when $\nu r_{\mathrm{UH}} \gtrsim |\mathrm{v}_g|$

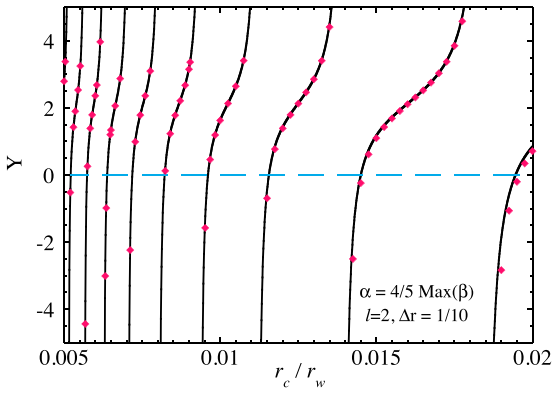

FIG. 9. Admittance versus cyclotron radius at fixed frequency and uniform $\alpha(r)$ profile, $\alpha = 4\beta_{\max}/5$, $\nu = 0$, and density given by Eq. (79). Dots: numerical solution of Eq. (85). Solid lines: WKB approximation, Eq. (151). Singularities in Y occur at the frequencies of Bernstein modes.

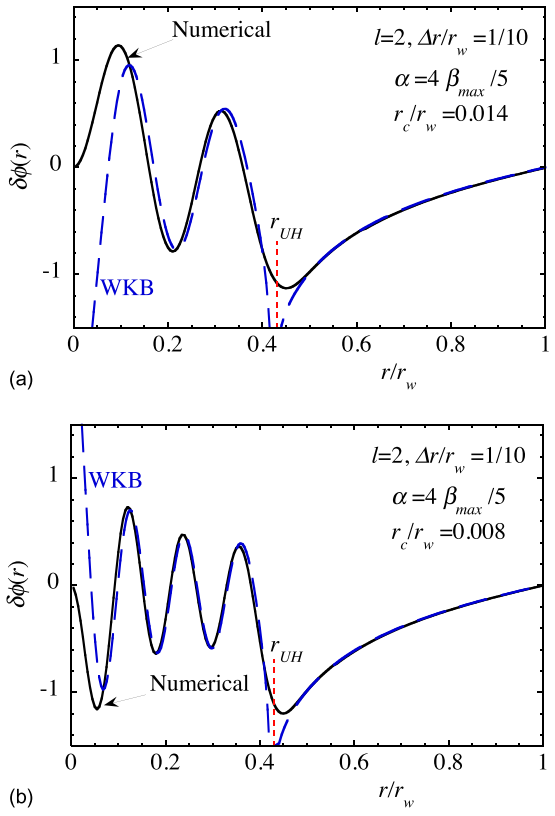

FIG. 10. Perturbed potential of $\ell = 2$ Bernstein modes for two different temperatures but the same frequency, and assuming uniform $\alpha(r)$, with $\alpha = 4\beta_{\max}/5$, and density given by Eq. (79). Solid lines: numerical solution of Eq. (85). Dashed lines: WKB approximation, Eqs. (147), (150), (138), (101), and (107). The dashed vertical line shows the location of the upper hybrid cutoff. (a) $r_c/r_w = 0.014$ and (b) $r_c/r_w = 0.008$. The WKB approximation improves for smaller r_c, and breaks down as expected near $r = 0$ and $r = r_{\mathrm{UH}}$.

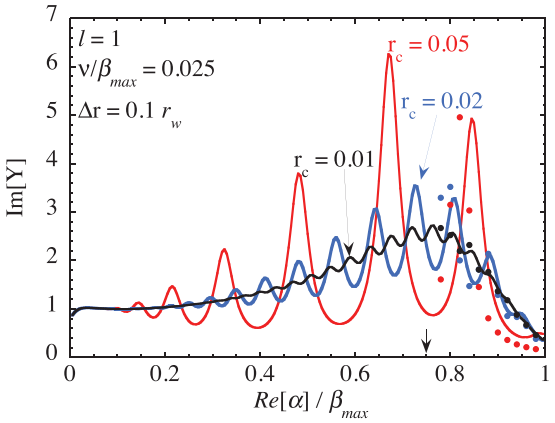

FIG. 11. Admittance versus frequency for uniform α, density given by Eq. (79), and $\nu = \beta_{\max}/40$ for $\ell = 1$, at three temperatures, with corresponding cyclotron radii r_c measured in units of r_w. As r_c decreases, the admittance approaches cold fluid theory, Eq. (70). For larger r_c, Bernstein mode peaks are evident. Curves: WKB theory given by Eq. (151), (138), and (127). Dots: numerical solution of Eq. (85), shown only in the regime of validity for Bernstein solutions of Eq. (85), $kr_c \ll 1$. The arrow at $\alpha/\beta_{\max} = 0.75$ shows the prediction of Eq. (77) for the frequency of the surface cyclotron wave.

[note that $|v_g|$ decreases as r_c decreases; see Eq. (107)]. In this regime, the Bernstein modes merge and disappear, and the cold-fluid limit is valid. Physically, the Bernstein waves are carrying energy away from the surface cyclotron wave and then damping due to collisions before normal modes can be set up.

1. Internal Bernstein modes with $\ell \le 0$

In addition to the Bernstein modes which occur for $\ell > 0$, there is a second set of Bernstein modes with $\ell \le 0$, related to the singular upper hybrid modes discussed in Sec. VI A. When there is no inner conductor, the $\ell \le 0$ Bernstein modes are purely internal modes, having no effect on the admittance. These Bernstein modes satisfy $\cos(\chi + \pi/4) = 0$, which implies $\chi = (n + 1/4)\pi$, for any integer n. Then, Eq. (142) implies that $A_L = A = 0$ and B_L is undetermined. Outside the plasma, $u = 0$.

Inside the plasma, $\delta\phi$ is given by Eq. (147) with $A_L = A = 0$. Outside, $\delta\phi$ is given by Eq. (149) with D_1 given in terms of B_L by Eqs. (118) and (119). Thus,

$$\delta\phi(r) = Cr^{-\ell} + \begin{cases} \dfrac{B_L}{k}\left(-\dfrac{2r_c\alpha}{rv_g}\right)^{1/2} \sin\left[\displaystyle\int_{r_{UH}}^{r} kdr + (n+1/4)\pi\right], & r < r_{UH} \\ -B_L\sqrt{\dfrac{\pi\mathcal{L}r_c}{r_{UH}}}(-1)^n\left(\dfrac{r_{UH}}{r}\right)^{\ell}, & r > r_{UH}. \end{cases} \tag{154}$$

For $\ell \le 0$, C can be chosen arbitrarily. By taking $C = B_L\sqrt{\pi\mathcal{L}r_c/r_{UH}}\, r_{UH}^{\ell}(-1)^n$, the perturbed potential outside the plasma vanishes. The result is an internal Bernstein mode with arbitrary amplitude B_L. The mode has no effect on the admittance; it can neither be detected nor launched using wall potentials. These modes have similar appearance to the $\ell > 0$ Bernstein modes, except that $\delta\phi = 0$ outside the plasma. The dispersion relation is given by $\chi = (n + 1/4)\pi$, which implies, using Eq. (138),

$$\int_0^{r_{UH}} kdr = \ell\frac{\pi}{2} + n\pi\,. \tag{155}$$

The frequencies predicted by Eq. (155) [using the general form for $k(\alpha/\beta)$ found by solving Eq. (127)] are shown in Fig. 12 for $\ell = 0$ and compared to the frequencies obtained from numerical solution of Eq. (85), again taking Eq. (79) as the species s density profile with $\Delta r = 1/10\, r_w$, and α uniform in r. There is good agreement with Eq. (85) solutions when $kr_c \ll 1$ (the lowest-order modes), and frequencies show the expected behavior given by Eq. (127) as wavenumber increases. A few of the low-order modes are displayed in Fig. 13.

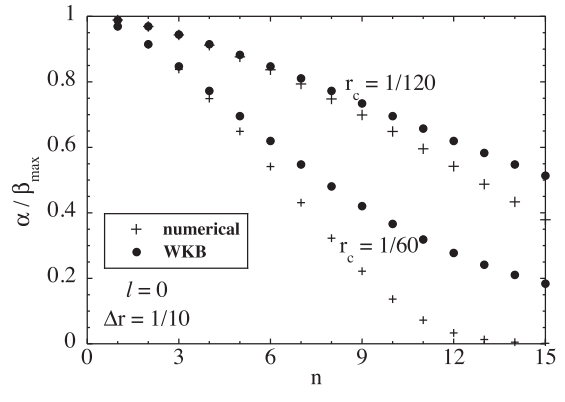

FIG. 12. Frequency spectrum of internal $\ell = 0$ Bernstein modes for two values of the cyclotron radius (measured in units of r_w). Plasma parameters are chosen, so that there is a single cutoff: the $\alpha(r)$ profile is assumed to be uniform, and density is given by Eq. (79). Crosses: numerical solution of Eq. (85), valid for the low order modes with $kr_c \ll 1$. Dots: WKB approximation, Eq. (155), valid for $k\mathcal{L} > 1$.

B. Two upper hybrid cutoffs

There are circumstances where the α and β profiles have the form shown in Fig. 14. For instance, in a centrifugally separated plasma, the density of a species of intermediate mass may have the form shown while the overall density is uniform, so that α is roughly constant;[25] see Fig. 1. There is then a range of frequencies for which there are two upper hybrid cutoffs, at radii r_{UH_1} and r_{UH_2}, $r_{UH_1} < r_{UH_2}$. The Bernstein dispersion relations are modified by the second cutoff.

In between the cutoffs, the WKB solution for $u(r)$ can be written in two equivalent ways,

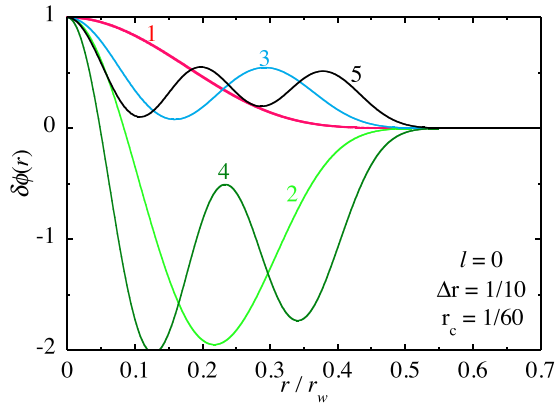

FIG. 13. The five lowest order internal Bernstein potential eigenmodes for $\ell = 0$ for the same plasma parameters as in Fig. 12, taking $r_c = 1/60$.

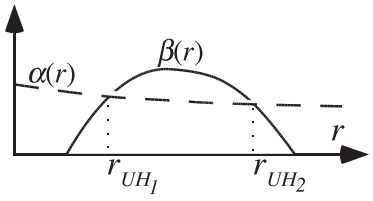

FIG. 14. α and β profiles for a case with two upper hybrid cutoffs.

$$u(r) = A\left[\frac{r^{\ell-1}}{D} + \frac{r_{\mathrm{UH}_2}^{\ell-1/2}}{\cos(\chi_2+\pi/4)} \times \left(-\frac{2\pi\mathcal{L}_2\alpha}{r\mathrm{v}_g}\right)^{1/2}\cos\left(\int_{r_{\mathrm{UH}_2}}^{r} k dr + \chi_2\right)\right] \quad (156)$$

or

$$u(r) = A\left[\frac{r^{\ell-1}}{D} + \frac{r_{\mathrm{UH}_1}^{\ell-1/2}}{\cos(\chi_1-\pi/4)} \times \left(\frac{-2\pi\mathcal{L}_1\alpha}{r\mathrm{v}_g}\right)^{1/2}\cos\left(\int_{r_{\mathrm{UH}_1}}^{r} k dr + \chi_1\right)\right], \quad (157)$$

where $\mathcal{L}_1^{-1} = |D'(r_{\mathrm{UH}_1})|$ and $\mathcal{L}_2^{-1} = D'(r_{\mathrm{UH}_2})$. These solutions must match, and therefore we require that the phases χ_1 and χ_2 satisfy

$$\chi_1 = \chi_2 - \int_{r_{\mathrm{UH}_1}}^{r_{\mathrm{UH}_2}} k\, dr, \quad (158)$$

and also

$$\cos(\chi_2+\pi/4) = \left(\frac{r_{\mathrm{UH}_2}}{r_{\mathrm{UH}_1}}\right)^{\ell-1/2}\sqrt{\frac{\mathcal{L}_2}{\mathcal{L}_1}}\cos(\chi_1-\pi/4)\,. \quad (159)$$

The perturbed potential then follows from Eq. (69). We must now integrate over the intermediate form, Eq. (113), at both r_{UH_1} and r_{UH_2}, to obtain the following WKB result for $\delta\phi(r)$:

$$\delta\phi = Cr^{-\ell} + Ar^{-\ell}\mathcal{P}\int_0^r \frac{dr' r'^{2\ell-1}}{D(r')} + A\begin{cases} 0\,, & r < r_{\mathrm{UH}_1} \\ -\pi\mathcal{L}_1 r_{\mathrm{UH}_1}^{2\ell-1}\tan\left(\chi_1-\frac{\pi}{4}\right)r^{-\ell} + \dfrac{r_{\mathrm{UH}_1}^{\ell-1/2}}{k\cos\left(\chi_1-\frac{\pi}{4}\right)} \\ \times\left(\dfrac{-2\pi\mathcal{L}_1\alpha}{r\mathrm{v}_g}\right)^{1/2}\cos\left(\displaystyle\int_{r_{\mathrm{UH}_1}}^{r} k dr + \chi_1\right), & r_{\mathrm{UH}_1} < r < r_{\mathrm{UH}_2} \\ \pi\left[\mathcal{L}_2 r_{\mathrm{UH}_2}^{2\ell-1}\tan\left(\chi_2+\frac{\pi}{4}\right) - \mathcal{L}_1 r_{\mathrm{UH}_1}^{2\ell-1}\tan\left(\chi_1-\frac{\pi}{4}\right)\right]r^{-\ell}, & r > r_{\mathrm{UH}_2}. \end{cases} \quad (160)$$

The Bernstein modes with $\ell > 0$ have $C = 0$ and satisfy $\delta\phi(r_w) = 0$, which implies the WKB dispersion relation

$$\int_0^{r_w}\mathcal{P}dr'\frac{r'^{2\ell-1}}{D(r')} + \pi\left[\mathcal{L}_2 r_{\mathrm{UH}_2}^{2\ell-1}\tan\left(\chi_2+\frac{\pi}{4}\right) - \mathcal{L}_1 r_{\mathrm{UH}_1}^{2\ell-1}\tan\left(\chi_1-\frac{\pi}{4}\right)\right] = 0. \quad (161)$$

The Bernstein modes with $\ell \le 0$ have $C \neq 0$ and satisfy $A = 0$ and $\cos(\chi_1-\pi/4) = 0 = \cos(\chi_2+\pi/4)$ [but $A/\cos(\chi_1-\pi/4)$ finite], which by Eq. (158) requires

$$\int_{r_{\mathrm{UH}_1}}^{r_{\mathrm{UH}_2}} k\, dr = (n-1/2)\pi \quad (162)$$

for any integer n.

C. Admittance regimes for the $\ell > 0$ cyclotron response in a single-species plasma

For a single species plasma with a monotonically decreasing density profile, the driven response to a wall potential with given mode number ℓ at a real frequency near the cyclotron frequency exhibits several regimes that depend on the locations of cutoffs and resonances. These in turn depend on the α and β profiles.

For $\ell \le 0$, the only possible plasma excitations are internal Bernstein modes (unless there is an inner conductor as in Sec. VI C). Furthermore, the $\alpha(r)$ profile for $\ell \le 0$ has the form shown in Fig. 15(b): it is monotonically decreasing in r. A cutoff, if one occurs, now traps the modes on the outside of the plasma. In this case, there will also generally be a resonance which will cause strong absorption unless the plasma edge is sharp compared to k, so that a reflection at the edge can occur. In any case, the $\ell \le 0$ excitations have no effect on the admittance because they are internal modes.

For $\ell > 1$, the $\alpha(r)$ profile has a typical form shown in Fig. 15(b); it may be non-monotonic, depending on the sharpness of the edge in the density profile, and the value of ℓ. Cutoffs and resonances occur in various locations depending on the frequency and mode number.

For $\ell > 1$, the different regimes are

1. $\omega - \Omega_c > (\ell - 1)\beta_{max}$ or $\omega - \Omega_c < (\ell - 1)\omega_E(r_w)$: Fluid regime

In this regime there are no resonances or cutoffs, so the admittance should be nearly that of a cold fluid plasma (Sec. IV); see Eq. (75).

2. $(\ell - 2)\beta_{max} + \Delta\alpha < \omega - \Omega_c < (\ell - 1)\beta_{max}$: Bernstein mode regime

Here, $\Delta\alpha$ is the depth of the minimum in $\alpha(r)$ (if a minimum exists–see Fig. 15(b)). In this regime, there is a single upper hybrid cutoff, so the admittance is as described in Sec. IX A: it displays peaks at the Bernstein mode frequencies, whose widths vanish as collisional damping ν vanishes; see Eq. (151).

3. $(\ell - 1)\omega_E(r_w) < \omega - \Omega_c < (\ell - 2)\beta_{max} + \Delta\alpha$: Resonance regime

In this regime there are one or possibly two resonances, along with a cutoff at larger radius. At the cutoff, the cold fluid solution (driven by the wall potential) couples to a Bernstein wave. This wave then carries energy to the nearest resonance, where it is absorbed via one of the processes mentioned in Sec. VIII B. Thus, the solution for $u(r)$ to the right of the cutoff is Eq. (66), and to the left (but away from the resonance) it is

$$u = \frac{Ar^{\ell-1}}{D} + B\left(\frac{-2r_c\alpha}{rv_g}\right)^{1/2} e^{i\int_{r_{UH}}^{r} kdr}. \tag{163}$$

Here, the positive sign in the exponential is chosen because the group velocity, given by Eq. (107), will then be negative, carrying energy to smaller radii according to Eq. (96). Furthermore, the coefficients B and A are related by the connection formulae (124)–(126) where, comparing Eq. (163) (calculated near the cutoff where $kr_c \to 0$) to (110), we find

$$\begin{aligned} B_L \cos\chi &= B, \\ B_L \sin\chi &= -iB, \\ A_L &= A. \end{aligned} \tag{164}$$

Then taking $B_{R_1} = 0$ in Eqs. (125) and (126) and solving for B yields

$$B = (1 - i)\sqrt{\frac{\pi\mathcal{L}}{2r_c}}\, r_{UH}^{\ell - 1/2} A\,. \tag{165}$$

The perturbed potential to the right of the cutoff is still given by Eq. (149), where D_1 is related to A through Eqs. (118), (119), (164), and (165)

$$D_1 = (1 - i)\sqrt{\frac{\pi}{2r_{UH}}}\left(\frac{\mathcal{L}}{r_c}\right)^{1/6} B = -i\pi\left(\frac{\mathcal{L}}{r_c}\right)^{2/3} r_{UH}^{\ell-1} A\,. \tag{166}$$

When this expression for D_1 is used in Eq. (149), and that expression for $\delta\phi(r)$ is used to determine the admittance via Eq. (75), the result is

$$Y = -\ell + r_w^{2\ell} \Bigg/ \left(\mathcal{P}\int_0^{r_w} dr' \frac{r'^{2\ell-1}}{D(r')} - \pi i \mathcal{L}\, r_{UH}^{2\ell-1} \right), \tag{167}$$

which is identical to the cold fluid result for a single cutoff, Eq. (78). In both cases, Bernstein waves carry energy away from the surface wave and damp before normal modes can be set up. In Eq. (78), the damping is due to collisions, but here the damping is also caused by absorption at the resonance.

Figure 16 plots the predicted admittance versus frequency for a single-species density profile of the form shown in Fig. 15, $\ell = 4$ and $\nu = \beta_{max}/100$. We use the general form for $k(\alpha/\beta)$ found by solving Eq. (127), and we use Eq. (167) in the resonance regime, and Eq. (151) in the Bernstein mode regime. For the parameters of the figure, these regimes are delineated by $0.66 \le (\omega - \Omega_c)/\beta_{max} \le 2$ and $2 \le (\omega - \Omega_c)/\beta_{max} \le 3$, respectively. Numerical solutions of Eq. (85) are also shown for values of ω that satisfy $kr_c \ll 1$. Peaks in the admittance due to weakly damped Bernstein modes are apparent, but the peaks disappear in the resonance regime where strong absorption of the Bernstein waves is predicted.

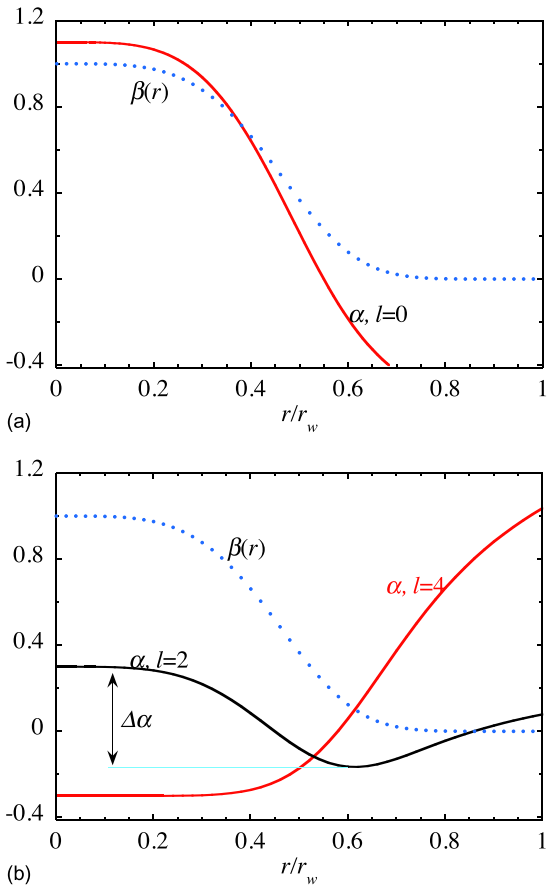

FIG. 15. β and representative α profiles (in units of β_{max}) for a single species plasma with monotonically decreasing density $n(r) = n_0 \exp(-(2r/r_w)^4)$. Frequencies are chosen so that there is one cutoff and one or more resonances. (a) $\ell \le 0$ and (b) $\ell > 1$.

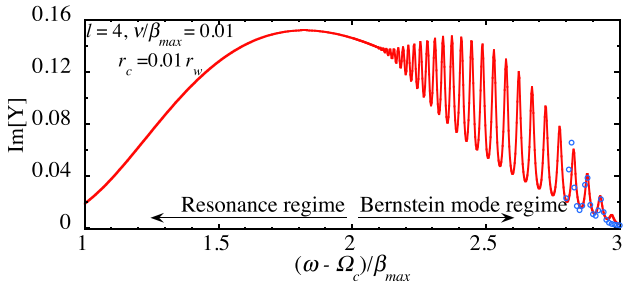

FIG. 16. Admittance versus frequency for an $\ell = 4$ wall perturbation in a single species plasma with the same plasma density as in Fig. 15, taking $r_c = r_w/100$ and $\nu = \beta_{\max}/100$. Curve: WKB solution. Dots: solution to Eq. (85).

X. CONCLUSIONS AND DISCUSSION

Two types of electrostatic cyclotron waves can propagate perpendicular to the magnetic field in a non-neutral plasma column: surface cyclotron waves and Bernstein waves. The surface cyclotron wave propagates only in the θ direction, causing density perturbations on the edge(s) of the column. These surface waves occur only for $\ell > 0$ in systems with no inner conductor, but can occur for any ℓ when there is an inner conductor. The waves can be launched and detected using electrodes at the wall, and are useful diagnostics of the various properties of different species such as their charge to mass ratio and concentration.

The Bernstein waves propagate both in r and θ, and their behavior is strongly influenced by resonances or cutoffs. At cutoffs, where the wave frequency equals the local upper hybrid frequency, the Bernstein waves are reflected, enabling normal modes. At resonances where the Doppler shifted wave frequency equals the cyclotron frequency as seen in the rotating frame, the Bernstein waves are absorbed.

In fusion plasmas, the method of cyclotron heating and current drive uses this resonance to heat and drive current the plasma, by absorbing applied electromagnetic wave energy.[27] However, in that case, the waves have finite k_z, which allows Landau damping via the "magnetic beach" process.[18] Here, where we consider waves with $k_z = 0$, spatial Landau damping can still occur, caused by $E \times B$ drift motion in the radial equilibrium electric field. However, as far as we know this has not been studied for Bernstein waves. More theory work is needed to elucidate this process. In addition, while we showed that the surface wave is not strongly affected by a resonance [because the field amplitude $u(r)$ passes through zero at resonance], there is probably some absorption caused by energy broadening of the cyclotron frequency $\bar{\Omega}$: see Eq. (19). This process will also be explored in future work.

Furthermore, we determined how Bernstein waves mode couple to the surface cyclotron wave at cutoffs. This coupling explains how the Bernstein waves can affect the admittance function (the normalized electric field at the wall). Energy from the surface cyclotron wave is coupled into the Bernstein waves, which damps and broadens the frequency response of the surface waves provided that the collision rate ν satisfies $\nu r_{\rm UH} \gtrsim |v_g|$. On the other hand, when $\nu r_{\rm UH} \lesssim |v_g|$, the coupling produces a set of sharp resonant peaks in the admittance due to Bernstein normal modes: see Figs. 11 and 16.

From the point of view of ion cyclotron mass spectrometry, the coupling of the surface wave to Bernstein modes and concomitant broadening of the admittance curve adds unwanted complexity to the plasma's frequency response. It may, therefore, be worthwhile to explore circumstances where a resonance wipes out the Bernstein mode response, while preserving a nearly undamped surface cyclotron wave. This occurred in the example of Fig. 4, where there is an inner conductor that allowed surface cyclotron waves to propagate, with no upper hybrid cutoff in the plasma. The use of an inner conductor allows this to occur in various cases (including $\ell > 0$ modes). This should be explored further.

Bernstein modes can also occur when $\ell \leq 0$ if there is a cutoff to reflect the waves and set up normal modes, but we found that (if there is no inner conductor) these waves are purely internal modes that make no potential perturbation outside the plasma (see Fig. 13, for example eigenfunctions). Furthermore, we find that resonances can damp these internal modes. Nevertheless, if there is a sufficiently sharp density gradient at the plasma edge, it has been shown in other work[24] that some of the low-order $\ell = 0$ modes with $k\mathcal{L} < 1$ can still occur. The damping process for these modes and its dependence on the plasma edge scale length $\mathcal{L}$ will be explored in future work.

Bernstein waves can also propagate at multiples of the cyclotron frequency. The methods used in this paper can be extended to investigate the behavior of these higher frequency Bernstein waves in a non-neutral plasma column. This issue will be pursued in future work.

Also, it is important to note that many experiments do not employ long plasma columns, and the theory presented here needs to be modified to account for finite length effects. One such effect that requires further study is the coupling of $\ell \leq 0$ internal modes to external electrodes at the end of the plasma column. This coupling should allow such modes to be detected and launched.

ACKNOWLEDGMENTS

The author thanks Professor C. F. Driscoll for useful discussions. This work was supported by National Science Foundation grant PHY-0903877, and Department of Energy Grants DE-SC0002451 and DE-SC0008693.

APPENDIX A: GUIDING CENTER HAMILTONIAN VIA CANONICAL LIE TRANSFORMATION

In this appendix, we outline the Lie transform perturbation method[14] used to derive Hamiltonian (3) from Eq. (1). This method is more elegant than using a perturbation method based on the mixed variable generating function W_r discussed in Sec. I. To prepare the Hamiltonian, we Taylor expand the effective potential $\phi_{\rm eff}(r)$ about the potential minimum at $r_0(p_\theta)$,

$$\begin{aligned}\phi_{\rm eff}(r) &= \phi_0(r) + \frac{1}{2mr^2}\left(p_\theta + \frac{qB}{2c}r^2\right)^2 \\ &= \phi_0(r_0) + \frac{\varepsilon^2}{2m\Omega_c^2}E^2(r_0) + \frac{\varepsilon^4}{m^2 r_0\Omega_c^4}E^3(r_0) \\ &\quad + \frac{1}{2}m\Omega^2(r_0)\delta r^2 + \frac{\varepsilon m\Omega_c^2}{r_0}\delta r^3 \\ &\quad \times\left(-\frac{1}{2} + \frac{2\varepsilon^2 E(r_0)}{m\Omega_c^2 r_0} - \frac{1}{6}\varepsilon^2\frac{E''(r_0)}{m\Omega_c^2}r_0\right) \\ &\quad + \frac{\varepsilon^2 m\Omega_c^2\delta r^4}{r_0^2}\left(\frac{5}{8} - \frac{5}{2}\frac{\varepsilon^2 E(r_0)}{m\Omega_c^2 r_0} - \frac{1}{24}\varepsilon^2 E'''(r_0)r_0^2\right) \\ &\quad - \frac{3}{4}\frac{\varepsilon^3 m\Omega_c^2\delta r^5}{r_0^3} + \frac{7}{8}\varepsilon^4\frac{m\Omega_c^2\delta r^6}{r_0^4} + O(\varepsilon^5)\,, \end{aligned} \tag{A1}$$

where $\delta r = r - r_0(p_\theta)$, and where we have used Eq. (4). A canonical transformation from r to δr is accomplished with a type-2 mixed generating function,

$$F_2(\mathbf{r},\mathbf{P}) = (r - r_0(P_\theta))\,P_r + \theta P_\theta, \tag{A2}$$

where capitalized momenta are the new momenta. This generator implies $p_r = P_r, p_\theta = P_\theta$, and it yields a new canonical angle coordinate Θ defined as

$$\Theta = \frac{\partial F_2}{\partial P_\theta} = \theta - \frac{\partial r_0}{\partial p_\theta}p_r. \tag{A3}$$

Next, we introduce lowest-order action-angle variables (ψ_0, μ_0) [and corresponding new conjugate coordinates (Θ_0, p_{θ_0})] using the usual definitions for the action-angle variables of a harmonic oscillator,

$$\delta r = \sqrt{\frac{2\mu_0}{m\Omega(r_0)}}\cos\psi_0, \quad p_r = -\sqrt{2\mu_0 m\Omega(r_0)}\sin\psi_0. \tag{A4}$$

The canonical transformation to these variables can be accomplished using a second generator $\bar{F}_2(\delta r, \Theta, \mu_0, p_{\theta_0})$ defined as

$$\begin{aligned}\bar{F}_2 &= -\frac{\delta r}{2}\sqrt{2m\Omega\mu_0 - m^2\Omega^2\delta r^2} \\ &\quad + \mu_0\cos^{-1}\left(\delta r\sqrt{\frac{m\Omega}{2\mu_0}}\right) + \Theta p_{\theta_0}. \end{aligned} \tag{A5}$$

This generator implies that $p_{\theta_0} = p_\theta$ and that

$$\Theta_0 = \frac{\partial F_2}{\partial p_{\theta_0}} = \Theta - \frac{\partial\Omega/\partial p_\theta}{2\Omega}\mu_0\sin 2\psi_0. \tag{A6}$$

When written in these coordinates, the Hamiltonian has the form

$$\begin{aligned}H_\perp(\psi_0,\mu_0,p_\theta) &= \mu_0\Omega(r_0) + \phi_0(r_0) + \frac{\varepsilon^2}{2m\Omega_c^2}E^2(r_0) \\ &\quad + \frac{\varepsilon^4}{m^2 r_0\Omega_c^2}E^3(r_0) + \varepsilon H_1(\psi_0,\mu_0,p_\theta) \\ &\quad + \varepsilon^2 H_2(\psi_0,\mu_0,p_\theta) + \cdots, \end{aligned} \tag{A7}$$

where

$$H_1 = -\sqrt{\frac{2\mu_0^3\Omega}{m}}\frac{\cos^3\psi_0}{r_0}, \tag{A8}$$

and $H_2, H_3, \ldots$ are not displayed due to their complexity.

The terms in $H_\perp$ involving ψ_0 are transformed away order-by-order using infinitesimal Lie transformations[13,14] from coordinates $\mathbf{z} = (\psi_0, \mu_0, \Theta_0, p_\theta)$ to new conjugate coordinates $\mathbf{Z} = (\psi, \mu, \bar{\theta}, \bar{p}_\theta)$. The transformation is generated by the following operator, defined by its action on a phase function $f(\mathbf{z})$:

$$\hat{T}f = \sum_{n=0}^{M}\frac{(-\varepsilon)^n}{n!}\hat{w}_n f. \tag{A9}$$

The operators $\hat{w}_n$ are defined recursively in terms of their action on f,

$$\hat{w}_n f = [\hat{w}_{n-1}f, g]\,, \quad \hat{w}_0 = 1, \tag{A10}$$

where $[\,,\,]$ is the Poisson bracket for the phase space and g is the generator of the transformation. Like $\hat{T}$, g is also written as a series in ε,

$$g = \sum_{n=1}^{M}\varepsilon^{n-1}g_n(\mathbf{z}). \tag{A11}$$

A new Hamiltonian $K(\mathbf{Z})$ is then obtained as a power series in ε via

$$K = \hat{T}\,H_\perp. \tag{A12}$$

The generators g_n are chosen to remove the ψ-dependence from the Hamiltonian, order-by-order in ε. Writing $K = K_0 + \varepsilon K_1 + \cdots$ and expanding Eq. (A12) in ε implies

$$\begin{aligned}&K_0 = \mu\Omega \equiv H_0, \\ &K_1 = H_1 - [H_0, g_1], \\ &K_2 = H_2 - [H_0, g_2] - [H_1, g_1] + \frac{1}{2}[[H_0, g_1], g_1] \\ &\quad\vdots \end{aligned} \tag{A13}$$

Also, coordinates are transformed according to

$$\mathbf{z} = \hat{T}\,\mathbf{Z} = \mathbf{Z} - \varepsilon[\mathbf{Z}, g_1] + O(\varepsilon^2). \tag{A14}$$

Note that since H_n is independent of Θ_0, so are g_n and K. Then, no derivatives of g_n with respect to $\bar{\theta}$ or $\bar{p}_\theta$ appear in Eqs. (A13). Also, Eq. (A14) then implies that $p_\theta = \bar{p}_\theta$.

At first order in ε, Eq. (A13) implies that $K_1 = 0$ and

$$\Omega\frac{\partial g_1}{\partial\psi} = -H_1(\psi,\mu,p_\theta), \tag{A15}$$

which may be solved for g_1 by integration. The constant of integration is chosen so that g_1 is periodic in ψ. Then, Eq. (A14) implies that

$$\mu_0 = \mu + \varepsilon \frac{\partial g_1}{\partial \psi} + O(\varepsilon^2),$$
$$\psi_0 = \psi - \varepsilon \frac{\partial g_1}{\partial \mu} + O(\varepsilon^2), \tag{A16}$$
$$\Theta_0 = \bar{\theta} - \varepsilon \frac{\partial g_1}{\partial p_\theta} + O(\varepsilon^2).$$

Working to $O(\varepsilon^4)$, the result for the Hamiltonian is given in Eq. (3). Also, application of the series expressions (A14) [taken up to $O(\varepsilon^4)$] to Eqs. (A6), (A4), and (A3) yields Eqs. (13) and (14).

APPENDIX B: DERIVATION OF THE QUASI-EQUILIBRIUM DISTRIBUTION

In this Appendix, we outline the derivation of Eq. (24), the expression for the quasi-equilibrium distribution function f_{qe}. One elegant approach employs a novel gyro-averaged collision operator that keeps both short-range (Boltzmann) and long-range[28] collisions. This approach will be discussed in a separate publication.[29] Here, we employ a perturbation approach, adapted from Ref. 16. The collision operator is assumed to be a Boltzmann operator. Equation (22) is transformed from coordinates $(r, \mathbf{v})$ to new coordinates $(r, \mathrm{v}_\perp, \psi_0, \mathrm{v}_z)$, where

$$\mathrm{v}_r = \mathrm{v}_\perp \cos\psi_0, \quad \bar{\mathrm{v}}_\theta = \mathrm{v}_\perp \sin\psi_0, \quad \mathrm{v}_r = \mathbf{v}\cdot\hat{r},$$
$$\bar{\mathrm{v}}_\theta = \mathbf{v}\cdot\hat{\theta} - \varepsilon \mathrm{v}_d(r,t) \tag{B1}$$

and the drift velocity v_d is defined by the solution of the quadratic equation

$$\frac{\mathrm{v}_d^2}{r} + \frac{E}{m} - \frac{\Omega_c}{\varepsilon}\mathrm{v}_d = 0. \tag{B2}$$

In these coordinates, Eq. (22) becomes

$$\frac{\partial f}{\partial t} - \varepsilon \frac{\partial \mathrm{v}_d}{\partial t}\left(\sin\psi_0 \frac{\partial}{\partial \mathrm{v}_\perp} + \frac{\cos\psi_0}{\mathrm{v}_\perp}\frac{\partial}{\partial \psi_0}\right) f + \mathrm{v}_\perp \cos\psi_0 \frac{\partial f}{\partial r}$$
$$- \varepsilon r \mathrm{v}_\perp \cos\psi_0 \frac{\partial}{\partial r}\left(\frac{\mathrm{v}_d}{r}\right)\left(\sin\beta \frac{\partial}{\partial \mathrm{v}_\perp} + \frac{\cos\psi_0}{\mathrm{v}_\perp}\frac{\partial}{\partial \psi_0}\right) f$$
$$+ \left(\frac{\Omega_c}{\varepsilon} - 2\varepsilon\frac{\mathrm{v}_d}{r} - \frac{\mathrm{v}_\perp}{r}\sin\psi_0\right)\frac{\partial f}{\partial \psi_0} = C(f,f). \tag{B3}$$

The solution for f is obtained as a power series in ε and $\hat{\nu} \equiv \nu\varepsilon/\Omega_c$, where ν is the collision frequency [a frequency scale factor on the order of $C(f,f)/f$]:

$$f = \sum_{\substack{n=0 \\ m=0}}^{\infty} \varepsilon^n \hat{\nu}^m f_{nm}. \tag{B4}$$

It was determined in Ref. 16 that $\partial/\partial t$ is of order $\hat{\nu}\varepsilon^3$, assuming that $\partial T/\partial r$ is of order ε^2 and $\partial n/\partial r$ is $O(1)$. For the quasi-equilibrium, we therefore are concerned with terms of order $\hat{\nu}^0$, i.e., f_{n0}.

The lowest order equation is

$$\frac{\Omega_c}{\varepsilon}\frac{\partial f_{00}}{\partial \psi_0} = 0, \tag{B5}$$

which implies that $f_{00} = f_{00}(r, \mathrm{v}_\perp, \mathrm{v}_z, t)$. The equation of order $\varepsilon^0\hat{\nu}^1$ is

$$\nu \frac{\partial f_{01}}{\partial \psi_0} = C(f_{00}, f_{00}). \tag{B6}$$

Averaging both sides over ψ_0 from 0 to 2π, and noting that f_{01} is periodic in ψ_0, implies that $C(f_{00}, f_{00}) = 0$, which implies that f_{00} is a local Maxwellian,

$$f_{00} = n(r,t)\left(\frac{m}{2\pi T(r,t)/m}\right)^{3/2} e^{-m\mathrm{v}^2/2T(r,t)}. \tag{B7}$$

Since $C(f_{00}, f_{00}) = 0$, Eq. (B6) then implies that $f_{01} = f_{01}(r, \mathrm{v}_\perp, \mathrm{v}_z, t)$. This function is determined at next order in $\hat{\nu}$

$$\nu \frac{\partial f_{02}}{\partial \psi_0} = \bar{C}(f_{00}, f_{01}), \tag{B8}$$

where $\bar{C}(f,g) \equiv C(f,g) + C(g,f)$. A ψ_0 average then implies that $\bar{C}(f_{00}, f_{01}) = 0$. However, this implies that $f_{01} = (A(r,t) + B(r,t)\mathrm{v}_z + C(r,t)\mathrm{v}^2) f_{00}$ (the collision operator conserves particle number, parallel momentum, and kinetic energy). When f_{01} is added to f_{00}, this merely redefines $n(r,t)$ and $T(r,t)$ (and allows a v_z drift which we ignore), so we can set $f_{01} = 0$.

Next we consider f_{10}, which must satisfy

$$\Omega_c \frac{\partial f_{10}}{\partial \psi_0} + \mathrm{v}_\perp \cos\psi_0 \frac{1}{n}\frac{\partial n}{\partial r} f_{00} = 0 \tag{B9}$$

[where we have used $\partial T/\partial r = O(\varepsilon^2)$]. The solution for f_{10} is

$$f_{10} = h_{10}(r, \mathrm{v}_\perp, \mathrm{v}_z, t) - \frac{\mathrm{v}_\perp}{\Omega_c}\sin\psi_0 \frac{1}{n}\frac{\partial n}{\partial r} f_{00}. \tag{B10}$$

The function h_{10} is determined using the equation of order $\varepsilon^1\hat{\nu}^1$,

$$\nu \frac{\partial f_{11}}{\partial \psi_0} = \bar{C}(f_{00}, h_{10}) - \frac{1}{\Omega_c n}\frac{\partial n}{\partial r}\bar{C}(f_{00}, \mathrm{v}_\perp \sin\psi_0 f_{00}). \tag{B11}$$

In Ref. 16, it is shown that the second term on the rhs vanishes due to conservation of momentum during collisions. Then, a ψ_0 average implies that $\bar{C}(f_{00}, h_{10}) = 0$, which implies, as before, that we may set $h_{10} = 0$, and we may set $f_{11} = 0$.

In Ref. 16, working to higher order, similar arguments were used to obtain f_{20},

$$f_{20} = h_{20}(r, \mathrm{v}_z, \mathrm{v}_\perp, t) + \frac{K(r,t)}{4\Omega_c^2}\mathrm{v}_\perp^2 \cos 2\psi_0 f_{00}, \tag{B12}$$

where

$$h_{20} = \frac{1}{4\Omega_c^2}\left(\frac{1}{n}\frac{\partial n}{\partial r}\right)^2 \left(\mathrm{v}_\perp^2 - \frac{2T}{m}\right) f_{00} \tag{B13}$$

and

$$K(r,t) = -\frac{1}{n}\frac{\partial^2 n}{\partial r^2} + \frac{1}{rn}\frac{\partial n}{\partial r} + \frac{m\Omega_c}{T} r \frac{\partial}{\partial r}\left(\frac{\mathrm{v}_d}{r}\right). \tag{B14}$$

Also, f_{21} was determined to be

$$\nu f_{21} = \frac{M(r,t)}{8\Omega_c^2}\bar{C}(f_{00}, \mathrm{v}_\perp^2 \sin 2\psi_0 f_{00}), \tag{B15}$$

where

$$M = -r\frac{\partial}{\partial r}\left(\frac{1}{rn}\frac{\partial n}{\partial r} - \frac{m\Omega_c}{T}\frac{\mathrm{v}_d}{r}\right). \tag{B16}$$

Finally, an expression for f_{30} was also obtained,

$$\begin{aligned} f_{30} = h_{30}(r,\mathrm{v}_z,\mathrm{v}_\perp,t) &- \frac{\mathrm{v}_\perp}{\Omega_c}\sin\psi_0 f_{00}\left\{\frac{m\mathrm{v}^2}{2T^2}\frac{\partial T}{\partial r} + \frac{\mathrm{v}_\perp^2}{4\Omega_c^2 n}\frac{\partial}{\partial r}\left[\frac{1}{n}\left(\frac{\partial n}{\partial r}\right)^2\right] + \frac{\mathrm{v}_\perp^2}{8\Omega_c^2 n}\frac{1}{r^2}\frac{\partial}{\partial r}r^2 nK - \frac{\mathrm{v}_\perp^2}{4\Omega_c}\frac{m}{T}r\frac{\partial}{\partial r}\left(\frac{\mathrm{v}_d}{r}\right)\frac{1}{n}\frac{\partial n}{\partial r}\right\} \\ &+ \frac{\mathrm{v}_\perp}{\Omega_c}\sin\psi_0 f_{00}\left\{\frac{3}{2T}\frac{\partial T}{\partial r} + \frac{T}{2\Omega_c^2 mn}\frac{\partial}{\partial r}\left[\frac{1}{n}\left(\frac{\partial n}{\partial r}\right)^2\right] - \frac{2\mathrm{v}_d}{\Omega_c rn}\frac{\partial n}{\partial r} - \frac{r}{\Omega_c n}\frac{\partial}{\partial r}\left(\frac{\mathrm{v}_d}{r}\right)\frac{\partial n}{\partial r}\right\} \\ &- \frac{\mathrm{v}_\perp^3}{\Omega_c n}\sin 3\psi_0 f_{00}\left[\frac{1}{24\Omega_c^2}\left(\frac{\partial}{\partial r} - \frac{2}{r}\right)(nK) + \frac{rm}{12\Omega_c T}\frac{\partial}{\partial r}\left(\frac{\mathrm{v}_d}{r}\right)\frac{\partial n}{\partial r}\right]. \end{aligned} \tag{B17}$$

However, the function h_{30} was not determined. Since we require f_{30}, we continue the derivation, using the $O(\varepsilon^3\hat{\nu}^1)$ equation

$$\begin{aligned} &\nu\left[\frac{\partial f_{31}}{\partial\psi_0} - \frac{\mathrm{v}_\perp}{\Omega_c r}\sin\psi_0\frac{\partial f_{21}}{\partial\psi_0} + \frac{\mathrm{v}_\perp\cos\psi_0}{\Omega_c}\frac{\partial f_{21}}{\partial r}\right] \\ &\quad = \bar{C}(f_{00},f_{30}) + \bar{C}(f_{10},f_{20}). \end{aligned} \tag{B18}$$

The function h_{30} is determined by integrating this equation over ψ_0. First, consider the terms involving f_{21}. To evaluate these, we note that the Boltzmann operator $\bar{C}(f,g)$ has the form

$$\begin{aligned} \bar{C}(f,g) = \int d^3\mathrm{v}_s d\Omega_s \sigma(\Omega_s,u)\, u[&f(\mathbf{v}')g(\mathbf{v}_s') + f(\mathbf{v}_s')g(\mathbf{v}') \\ &- f(\mathbf{v})g(\mathbf{v}_s) - f(\mathbf{v}_s)g(\mathbf{v})], \end{aligned} \tag{B19}$$

where $\sigma(\Omega_s,u)$ is the cross-section for scattering angle Ω_s, $u = |\mathbf{v} - \mathbf{v}_s|$ and the prime denotes post-collision velocities. For f_{21}, the collision integral involved in Eq. (B15) is

$$\begin{aligned} \bar{C}(f_{00}, \mathrm{v}_\perp^2\sin 2\psi f_{00}) = \int d^3\mathrm{v}_s d\Omega_s \sigma(\Omega_s,u)\, u f_{00}(\mathbf{v}) f_{00}(\mathbf{v}_s) \\ \times (\mathrm{v}_{\perp s}'^2\sin 2\psi_s' + \mathrm{v}_\perp'^2\sin 2\psi_0' \\ - \mathrm{v}_{\perp s}^2\sin 2\psi_s - \mathrm{v}_\perp^2\sin 2\psi_0), \end{aligned} \tag{B20}$$

where ψ_s is a variable of integration through $\mathbf{v}_s$, and ψ_0' and ψ_s' are variables of integration through their dependence on Ω_s. The operator has the following symmetry: if we define new angles via $\psi_s = \psi_0 + \Delta\psi_s, \psi_0' = \psi_0 + \Delta\psi'$ and $\psi_s' = \psi_0 + \Delta\psi_s'$, the operator

$$\int d^3\mathrm{v}_s d\Omega_s\, \sigma(\Omega_s,u)\, u f_{00}(\mathbf{v}) f_{00}(\mathbf{v}_s) \tag{B21}$$

is independent of ψ_0, by the isotropy of the collision process with respect to rotations about the z axis. This angle transformation transfers all ψ_0 dependence to the four sin terms in Eq. (B20), specifically $\sin(2\psi_0 + 2\Delta\psi_s')$, $\sin(2\psi_0 + \Delta\psi')$, $\sin(2\psi_0 + \Delta\psi_s)$, and $\sin 2\psi_0$. Therefore, f_{21} is a sum of two terms, one proportional to $\sin 2\psi_0$ and the other proportional to $\cos 2\psi_0$. This implies that

$$\int_0^{2\pi}\frac{d\psi_0}{2\pi}\sin\psi_0\frac{\partial f_{21}}{\partial\psi_0} = \int_0^{2\pi}\frac{d\psi_0}{2\pi}\cos\psi_0\frac{\partial f_{21}}{\partial r} = 0. \tag{B22}$$

A similar argument implies that

$$\int_0^{2\pi}\frac{d\psi_0}{2\pi}\bar{C}(f_{10},f_{20}) = 0 \tag{B23}$$

and that

$$\int_0^{2\pi}\frac{d\psi_0}{2\pi}\bar{C}(f_{00},f_{30}) = \bar{C}(f_{00},h_{30}). \tag{B24}$$

Thus, the ψ_0 average of Eq. (B18) implies that $\bar{C}(f_{00},h_{30}) = 0$, so we can set $h_{30} = 0$. Therefore, to $O(\varepsilon^3)$, the quasi-equilibrium distribution is

$$\begin{aligned} f_{qe} = f_{00} + \varepsilon f_{10} + \varepsilon^2 f_{20} + \varepsilon^3 f_{30} + O(\varepsilon^4) = \frac{n(r)}{(2\pi T/m)^{3/2}}\exp[-m\Delta\mathrm{v}^2/2T(r)]\left\{1 + \frac{\varepsilon^2 r\omega_{r_0}'}{4\Omega_c T}m(\mathrm{v}_r^2 - \Delta\mathrm{v}_\theta^2) + \varepsilon^3\Delta\mathrm{v}_\theta\right. \\ \left.\times\left[\frac{T'}{2\Omega_c T}\left(3 - \frac{m\Delta\mathrm{v}^2}{T}\right) - \frac{\omega_{r_0}'}{4\Omega_c^2 T}\left(m\left(\mathrm{v}_r^2 + \frac{5}{3}\Delta\mathrm{v}_\theta^2\right) + 2rT\frac{n'}{n}\right) - \frac{r\omega_{r_0}''}{4\Omega_c^2 T}m(\mathrm{v}_r^2 + \frac{1}{3}\Delta\mathrm{v}_\theta^2)\right]\right\} + O(\varepsilon^4), \end{aligned} \tag{B25}$$

where $\Delta v^2 = v_r^2 + v_z^2 + \Delta v_\theta^2$, $\Delta v_\theta = \mathbf{v} \cdot \hat{\theta} - \varepsilon r \omega_{r_0}$, and ω_{r_0} is the rotation frequency for a thermal equilibrium system,

$$\omega_{r_0}(r) = \frac{1}{m\Omega_c r}\left(E(r) - \frac{T(r)}{n(r)}n'(r)\right) + \frac{\omega_{r_0}^2(r)}{\Omega_c}. \qquad \text{(B26)}$$

When Eq. (B25) is multiplied by Δv_θ, integrated over $\mathbf{v}$, and divided by nr, one obtains a correction to this rotation frequency due to shears, given in Eq. (28).

This expression for f_{qe} can be converted into a function solely of the constants of motion, Eq. (24), by substituting Eqs. (9) and (13) for r, their time derivative for v_r [using Eq. (16)], and the time-derivative of Eqs. (11) and (14) for v_θ/r [using Eqs. (16) and (17)]. The result, in terms of r_0, v_z and μ, and independent of ψ, can be converted to Eq. (24) using Eq. (4).

[1]A. G. Marshall and C. L. Hendrickson, Int. J. Mass Spectrometry **215**, 59 (2002).
[2]E. Sarid, F. Anderegg, and C. F. Driscoll, Phys. Plasmas **2**, 2895 (1995).
[3]R. W. Gould and M. A. LaPointe, Phys. Fluids B **4**, 2038 (1992).
[4]G. Pearson, Phys. Fluids **9**, 2454 (1966).
[5]R. W. Gould and M. A. LaPointe, Phys. Rev. Lett. **67**, 3685 (1991).
[6]R. W. Gould, Phys. Plasmas **2**, 1404 (1995).
[7]T. H. Stix and D. G. Swanson, "Propogation and mode conversion for waves in nonuniform plasmas," in *Handbook of Plasma Physics*, edited by A. Galeev and R. Sudan (North-Holland, Amsterdam, 1983), Vol. 1.
[8]P. L. Colestock and R. J. Kashuba, Nucl. Fusion **23**, 763 (1983).
[9]A. K. Ram, A. Bers, S. Schultz, and V. Fuchs, Phys. Plasmas **3**, 1976 (1996).
[10]A. K. Ram and S. Schultz, Phys. Plasmas **7**, 4084 (2000).
[11]M. D. Tinkle and S. Barlow, J. Appl. Phys. **90**, 1612 (2001).
[12]R. S. Van Dyck, F. L. Moore, D. L. Farnham, and P. B. Schwinberg, Phys. Rev. A **40**, 6308 (1989).
[13]H. Goldstein, *Classical Mechanics*, 2nd ed. (Addison Wesley, Reading, Massachusetts, 1980).
[14]R. G. Littlejohn, J. Math. Phys. **20**, 2445 (1979).
[15]L. S. Brown and G. Gabrielse, Rev. Mod. Phys. **58**, 233 (1986).
[16]T. M. O'Neil and C. F. Driscoll, Phys. Fluids **22**, 266 (1979).
[17]D. H. E. Dubin and T. M. O'Neil, Rev. Mod. Phys. **71**, 87 (1999).
[18]T. H. Stix, *Waves in Plasmas* (American Institute of Physics, New York, 1992).
[19]D. E. Baldwin and D. W. Ignat, Phys. Fluids **12**, 697 (1969); D. H. E. Dubin, Phys. Plasmas **12**, 042107 (2005).
[20]P. Bellan, *Fundamentals of Plasma Physics* (Cambridge Univ. Press, Cambridge, 2006).
[21]I. S. Gradshteyn and I. M. Ryzhik, *Tables of Integrals, Series and Products* (American Institute of Physics, New York, 1980).
[22]R. C. Davidson, *Physics of Non-neutral Plasmas* (Addison-Wesley, New York, 1998), Eq. (4.226). Note that $\omega^+ - \omega^- \cong \Omega_c - 2\omega_E$.
[23]G. B. Whitham, *Linear and Nonlinear Waves* (John Wiley and Sons, New York, 1974), p. 383.
[24]G. W. Hart and R. L. Spencer, "Properties of axisymmetric Bernstein modes in an infinite length non-neutral plasma" (to be published).
[25]T. M. O'Neil, Phys. Fluids **24**, 1447 (1981).
[26]L. Rayleigh, *Scientific Papers* (Cambridge Univ. Press, Cambridge, 1899), Vol. 1, p. 474.
[27]N. J. Fisch, Rev. Mod. Phys. **59**, 175 (1987).
[28]D. H. E. Dubin, Phys. Plasmas **5**, 1688 (1998).
[29]D. H. E. Dubin, Phys. Plasmas (to be published).